

Wright State University

CORE Scholar

[Browse all Theses and Dissertations](#)

[Theses and Dissertations](#)

2013

The Solvent-Free Synthesis of and N-Methyl-N-Alkylpiperidinium Salts and Their Anion Exchange Reactions with Dilithium Phthalocyanine

Michael Joseph Krol Jr.
Wright State University

Follow this and additional works at: https://corescholar.libraries.wright.edu/etd_all

 Part of the [Chemistry Commons](#)

Repository Citation

Krol, Michael Joseph Jr., "The Solvent-Free Synthesis of and N-Methyl-N-Alkylpiperidinium Salts and Their Anion Exchange Reactions with Dilithium Phthalocyanine" (2013). *Browse all Theses and Dissertations*. 703.

https://corescholar.libraries.wright.edu/etd_all/703

This Thesis is brought to you for free and open access by the Theses and Dissertations at CORE Scholar. It has been accepted for inclusion in Browse all Theses and Dissertations by an authorized administrator of CORE Scholar. For more information, please contact library-corescholar@wright.edu.

THE SOLVENT-FREE SYNTHESIS OF N-METHYL-N-ALKYLPYPERIDIUM SALTS
AND THEIR ANION EXCHANGE REACTIONS WITH DILITHIUM
PHTHALOCYANINE

A thesis submitted in partial fulfillment
of the requirements for the degree of
Master of Science

By

Michael Joseph Krol Jr.
B.S., Loras College, 2011

2013
Wright State University

WRIGHT STATE UNIVERSITY

GRADUATE SCHOOL

April 16, 2013

I HEREBY RECOMMEND THAT THE THESIS PREPARED UNDER MY SUPERVISION BY Michael Joseph. Krol Jr. ENTITLED The Solvent-Free Synthesis of N-Methyl-N-Alkylpiperidium Salts and their Anion Exchange Reactions with Dilithium Phthalocyanine. BE ACCEPTED IN PARTIAL FULFILLMENT OF THE REQUIREMENTS FOR THE DEGREE OF Master of Science.

William A. Feld, Ph.D., Director
Department of Chemistry
College of Science and Mathematics

David A. Grossie, Ph.D., Chair
Department of Chemistry
College of Science and Mathematics

Committee on Final Examination

Eric Fossum, Ph.D.

David A. Grossie, Ph.D.

William A. Feld, Ph.D.

R. William Ayres, Ph.D.
Interim Dean, Graduate School

ABSTRACT

Krol, M. Joseph. M.S., Department of Chemistry, Wright State University, 2013. The Solvent-Free Synthesis of N-Methyl-N-Alkylpiperidinium Salts and their Anion Exchange Reactions with Dilithium Phthalocyanine.

A nucleophilic substitution reaction of N-methylpiperidine with bromopropane, bromobutane, bromopentane, bromohexane and bromoheptane was carried out in a Q-Tube with excess alkyl halide and yielded N-methyl-N-propylpiperidinium bromide, N-methyl-N-butylpiperidinium bromide, N-methyl-N-pentylpiperidinium bromide, N-methyl-N-hexylpiperidinium bromide and N-methyl-N-heptylpiperidinium bromide in yields from 85 to 92 %. The salts, which were solids at room temperature, were soluble in dichloromethane and were characterized by ^1H and ^{13}C NMR, elemental analysis and DSC. Two of the piperidinium bromides, N-methyl-N-propylpiperidinium bromide, N-methyl-N-butylpiperidinium bromide were used in an anion exchange reaction with dilithium phthalocyanine to yield N-methyl-N-propylpiperidinium lithium phthalocyanine and N-methyl-N-butylpiperidinium lithium phthalocyanine, respectively in 78 to 85% yield. The exchange products were soluble in dimethyl sulfoxide and were characterized by ^1H NMR, elemental analysis and TGA/DSC.

TABLE OF CONTENTS

	Page
INTRODUCTION	1
HISTORICAL.....	2
Ionic Liquid.....	2
Synthesis of Pyrrolidinium and Piperidinium based Ionic Liquids	2
Micelle Formation by N-alkyl-N-methylpiperidinium bromide Ionic Liquids	6
Ionic liquid Electrolyte for Electrochemical Application.....	6
Phthalocyanine.....	8
Usage of Phthalocyanine.....	8
Calculated Dilithium Phthalocyanine Structure.....	9
Crystal Structure of Dilithium Phthalocyanine.....	9
Exchange Reactions of Dilithium Phthalocyanine	11
EXPERIMENTAL.....	16
Instrumentation and Chemicals.....	16
General Procedure for the Reaction of N-methylpiperidine and 1-bromoalkanes ..	16
N-Methyl-N-propylpiperidinium Bromide (PIP ₁₃ Br) 1c	16
N-Methyl-N-butylpiperidinium Bromide (PIP ₁₄ Br) 1d	17
N-Methyl-N-pentylpiperidinium Bromide (PIP ₁₅ Br) 1e	17
N-Methyl-N-hexylpiperidinium Bromide (PIP ₁₆ Br) 1f	17

TABLE OF CONTENTS (CONTINUED)

	Page
N-Methyl-N-heptylpiperidinium Bromide (PIP ₁₇ Br) 1g	18
General Procedure for the preparation of N-alkyl-N-methylpiperidinium lithium phthalocyanines.....	18
N-Methyl-N-propylpiperidinium lithium phthalocyanine 21	18
N-Methyl-N-butylpiperidinium lithium phthalocyanine 22	19
RESULTS AND DISCUSSION.....	20
Elemental Analysis	21
Melting point.....	22
¹ H NMR Spectroscopy.....	23
¹³ C and Dept 135 NMR Spectroscopy	31
IR Spectroscopy	36
Thermal Gravimetric Analysis.....	40
Differential Scanning Calorimetry.....	41
CONCLUSIONS	48
REFERENCES	63
VITAE.....	65

LIST OF FIGURES

Figure	Page
1. The crystal structure of 2 as obtained by single crystal x-ray diffraction.	10
2. Melting points results	23
3. ¹ H NMR spectrum (CDCl ₃) of N-methylpiperidine 8	23
4. ¹ H NMR spectrum (CDCl ₃) of PIP ₁₃ Br 1c	24
5. ¹ H NMR spectrum (CDCl ₃) of PIP ₁₄ Br 1d	25
6. ¹ H NMR spectrum (CDCl ₃) of PIP ₁₅ Br 1e	26
7. ¹ H NMR spectrum (CDCl ₃) of PIP ₁₆ Br 1f	27
8. ¹ H NMR spectrum (CDCl ₃) of PIP ₁₇ Br 1g	28
9. ¹ H NMR spectrum (DMSO-d ₆) of PIP ₁₃ Br LiPc 21	29
10. ¹ H NMR spectrum (DMSO-d ₆) of PIP ₁₄ Br LiPc 22	30
11. ¹³ C and Dept 135 NMR spectra (CDCl ₃) of N-methylpiperidine 8	31
12. ¹³ C and Dept 135 NMR spectra (CDCl ₃) of PIP ₁₃ Br 1c	32
13. ¹³ C and Dept 135 NMR spectra (CDCl ₃) of PIP ₁₄ Br 1d	33
14. ¹³ C and Dept 135 NMR spectra (CDCl ₃) of PIP ₁₅ Br 1e	34
15. ¹³ C and Dept 135 NMR spectra (CDCl ₃) of PIP ₁₆ Br 1f	35
16. ¹³ C and Dept 135 NMR spectra (CDCl ₃) of PIP ₁₇ Br 1g	36
17. IR (NaCl plate) spectrum of PIP ₁₃ Br 1c	37
18. IR (NaCl plate) spectrum of PIP ₁₄ Br 1d	37
19. IR (NaCl plate) spectrum of PIP ₁₅ Br 1e	38

LIST OF FIGURES (CONTINUED)

Figure	Page
20. IR (NaCl plate) spectrum of PIP ₁₆ Br 1f	39
21. IR (NaCl plate) spectrum of PIP ₁₇ Br 1g	39
22. Weight % vs. temperature TGA overlay of 21 and 22	40
23. DSC trace of PIP ₁₃ Br 1c	41
24. DSC trace of PIP ₁₄ Br 1d	42
25. DSC trace of PIP ₁₅ Br 1e	43
26. DSC trace of PIP ₁₆ Br 1f	44
27. DSC trace of PIP ₁₇ Br 1g	45
28. DSC trace of PIP ₁₃ LiPc 21	46
29. DSC trace of PIP ₁₄ LiPc 22	47
30. 300 MHz ¹ H NMR spectrum (CDCl ₃) of 8	49
31. 75 MHz ¹³ C and Dept 135 NMR spectra (CDCl ₃) of 8	49
32. 300 MHz ¹ H NMR spectrum (CDCl ₃) of PIP ₁₃ Br 1c	50
33. 75 MHz ¹³ C and Dept 135 NMR spectra (CDCl ₃) of PIP ₁₃ Br 1c	50
34. IR (NaCl plate) spectrum of PIP ₁₃ Br 1c	51
35. DSC trace of PIP ₁₃ Br 1c	51
36. 300 MHz ¹ H NMR spectrum (CDCl ₃) of PIP ₁₄ Br 1d	52
37. 75 MHz ¹³ C and Dept 135 NMR spectra (CDCl ₃) of PIP ₁₄ Br 1d	52
38. IR (NaCl plate) spectrum of PIP ₁₄ Br 1d	53
39. DSC trace of PIP ₁₄ Br 1d	53
40. 300 MHz ¹ H NMR spectrum (CDCl ₃) of PIP ₁₅ Br 1e	54

LIST OF FIGURES (CONTINUED)

Figure	Page
41. 75 MHz ¹³ C and Dept 135 NMR spectra (CDCl ₃) of PIP ₁₅ Br 1e	54
42. IR (NaCl plate) spectrum of PIP ₁₅ Br 1e	55
43. DSC trace of PIP ₁₅ Br 1e	55
44. 300 MHz ¹ H NMR spectrum (CDCl ₃) of PIP ₁₆ Br 1f	56
45. 75 MHz ¹³ C and Dept 135 NMR spectra (CDCl ₃) of PIP ₁₆ Br 1f	56
46. IR (NaCl plate) spectrum of PIP ₁₆ Br 1f	57
47. DSC trace of PIP ₁₆ Br 1f	57
48. 300 MHz ¹ H NMR spectrum (CDCl ₃) of PIP ₁₇ Br 1g	58
49. 75 MHz ¹³ C and Dept 135 NMR spectra (CDCl ₃) of PIP ₁₇ Br 1g	58
50. 300 IR (NaCl plate) spectrum of PIP ₁₇ Br 1g	59
51. DSC trace of PIP ₁₇ Br 1g	59
52. 300 MHz ¹ H NMR spectrum (DMSO-d ₆) of PIP ₁₃ Br LiPc 21	60
53. 300 MHz ¹ H NMR spectrum (DMSO-d ₆) of PIP ₁₄ Br LiPc 22	60
54. TGA overlay of PIP ₁₃ LiPc 21 and PIP ₁₄ LiPc 22	61
55. DSC trace of PIP ₁₃ LiPc 21	61
56. DSC trace of PIP ₁₄ LiPc 22	62

LIST OF TABLES

Table	Page
1. Compounds numbers and abbreviation that been research	21
2. Elemental Analysis Results.	22
3. Melting point results	22

DEDICATION

I would like to dedicate this thesis to my parents, Michael and Lory Krol, my grandparents, Valeer and Alix Dumon and to my brother, Benjamin Krol. If it was not for their support and encouragement, this thesis would have been more difficult and taken a longer time to complete.

ACKNOWLEDGMENTS

I would like to thank my advisor Dr. William A. Feld for allowing me the opportunity to work in his research group. The guidance and experience, I received from him has helped me grow as a person and chemist.

I would like to thank my family and friends without them. I wouldn't be the person I am today without them. Also, I wouldn't have been able to finish my degree without their support.

Finally, I would like to thank the faculty, staff, and graduate students at Wright State Chemistry department for all the experiences over the past two year.

HISTORICAL

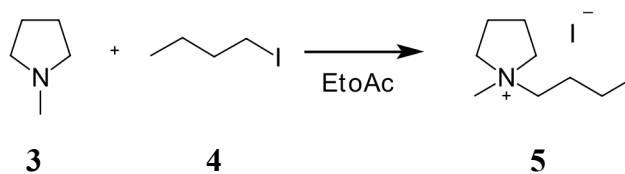
Ionic Liquids

Ionic liquids have become a highly researched topic due to the nature and properties of ionic liquids. Many focus on the potential of ionic liquids as solvents for industrial usage for catalytic reactions to make reactions more environmentally friendly. The definition generally given for ionic liquids is, "Ionic liquids are, quite simply, liquids that are comprised entirely of ions."¹ Some useful properties of ionic liquids are their thermal stability, negligible vapor pressure, high solubility in a range of inorganic and organic materials, inflammability and ease of preparation.

Ionic liquids have received the name designer solvents for their ability to be manipulated to optimize a reaction. Ionic liquids can vary by either the cation or anion. For example, by changing the anion size, the melting point can be increased or decreased. Similarly, changing the cation between organic and inorganic causes the same effect.¹ The characteristics of ionic liquids could allow industry to operate cleaner and more efficiently.

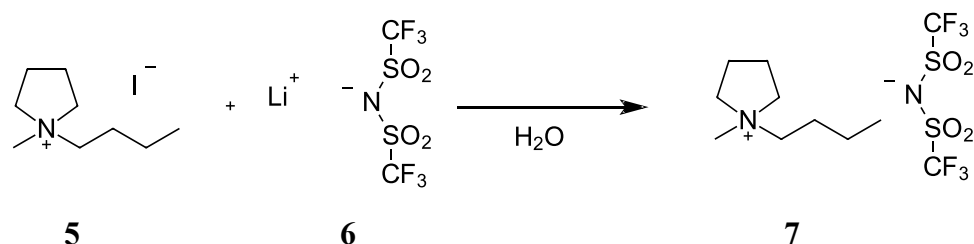
Synthesis of Pyrrolidinium and Piperidinium based Ionic Liquids

The reaction of N-methylpyrrolidine **3** and 1-iodobutane **4** provides N-butyl-N-methylpyrrolidinium iodide **5**. Environmentally friendly solvents like water and ethyl



acetate were used throughout the synthesis rather than solvents such as acetone and acetonitrile.

Salt **5** was used in the synthesis of N-butyl-N-methylpyrrolidinium bis(trifluoromethanesulfonyl)imide **7** by an exchange reaction with lithium bis(trifluoromethanesulfonyl)imide (LiTFSI) in water. The yield of **7** as a function of exchange time and stoichiometry were investigated.



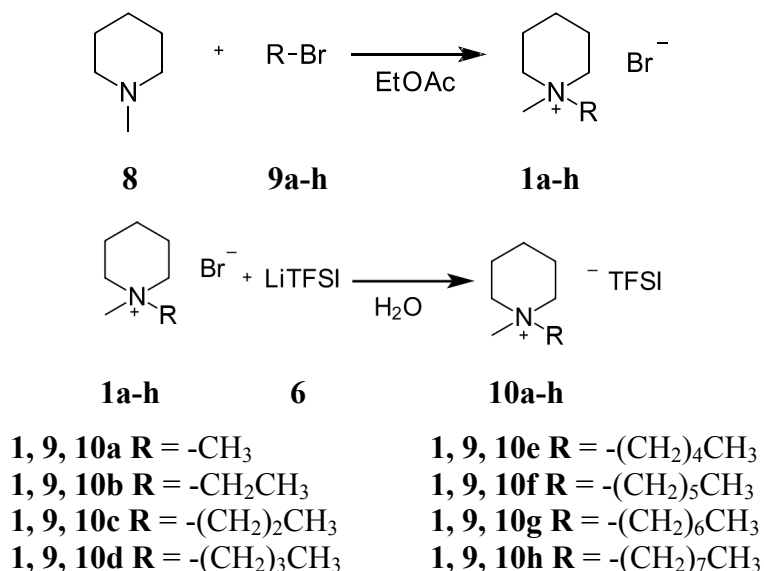
The effect of temperature and time were investigated. When the reaction was carried out at lower temperature (20° to 30°), the reaction required 24 hours to produce a yield of 95%. When the reaction temperature was increased to 45°, the time that was required to reach a yield of 100% was 5 hours.²

The yield of **7** was found to be dependent on exchange time. The yield was compared at 10 minutes and 1 hour. It was found that at 10 min. the product yield reached 85% and after 1 hour the yield stabilized around 95%. It was found that increasing the exchange time further had no practical increase in the product yield of **7**.²

Stoichiometry was also investigated. The effect of using **3** in excess was evaluated with two different reaction conditions (2 h at 50° and 5 h at 45°). When increasing the excess from 3 to 10 wt. % for **3**, the reaction resulted in an increase from 85% to 90% yield for the synthesis at 50° for 2 hr. and from 90% to 100% yield for the synthesis at 45° for 5 hr. The use of a higher molar excess of **3** has no practical effect on the yield. Excess **3** can be recycled by recovery from the ethyl acetate washings.²

The effect of using excess of **6** was also evaluated. An excess of **6** from 0 to 3% was used and resulted in a slight increase in the yield of **7** from 93.5 to 94.6%. Any further increase in the excess of **6** had a negative effect on yield. When an excess of **6** up to 30% was used, a decrease in yield was observed.²

The synthesis of cyclic alkyl quaternary ammonium cations based on the N-alkyl-N-methylpiperidinium bromides **1a-h** has been reported.³ They were investigated for their high thermal and electrochemical stabilities for use in electrochemical applications. The synthesis of **1a-h** bromide was carried out by reacting N-methylpiperidine **8** with bromomethane **9a**, bromoethane **9b**, 1-bromopropane **9c**, 1-bromobutane **9d**, 1-bromopentane **9e**, 1-bromohexane **9f**, 1-bromoheptane **9g** and 1-bromooctane **9h** in ethyl acetate. The corresponding TFSI salts, **10a-h**, were prepared by an exchange reaction of the bromides **9a-h** with **6** in water.

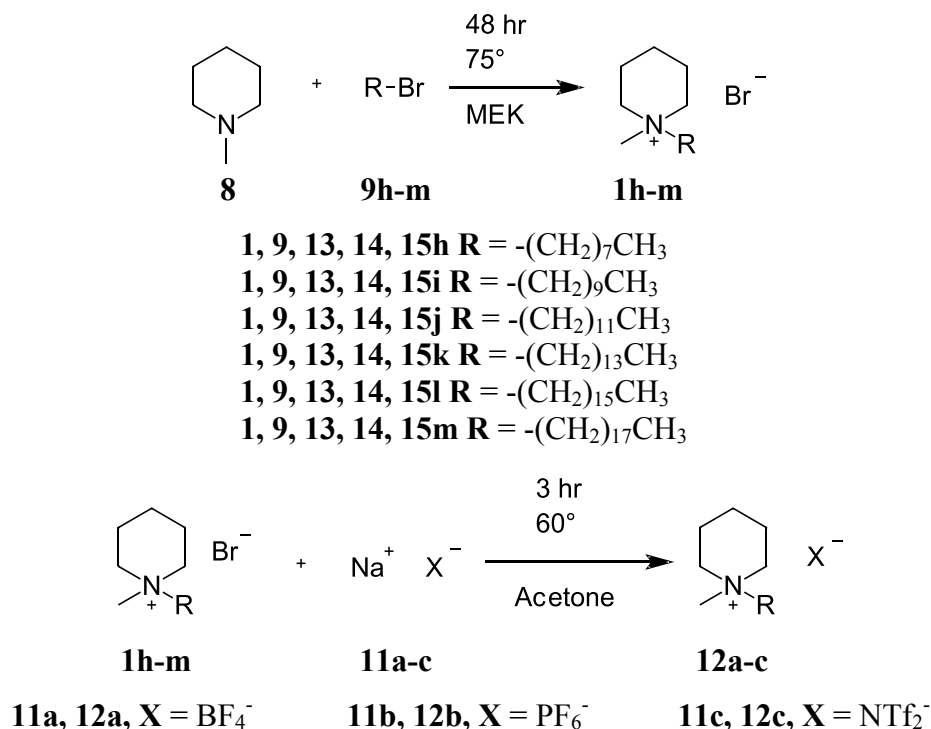


The alkyl chain length affected the melting point for **10a-h**; as the alkyl chain length increased the melting point decreased. The salts **10a-h** showed complex thermal behavior as shown by DSC. Some of the salts showed no crystalline phases, while others

showed a variable number of crystalline phases with a majority of those phases being endothermic.

It was observed that the ionic conductivity is dependent on temperature. When the alkyl chain increased from one carbon in **10a** to two carbons in **10b**, the conductivity increased about one order of magnitude. The other members of the series **10c-h** showed essentially the same conductivity as **10b**. Also, as the alkyl chain length increased, conductivity decreases occur at lower temperatures.³

A second related synthesis of N-alkyl-N-methylpiperidinium bromides **1h-m** explored unusual mesophases of ionic liquid crystals based on aliphatic heterocycles. The ionic liquid crystals were synthesized by reacting appropriate bromoalkanes **9h-m** with **8** in 2-butanone (MEK). The exchange products were synthesized by mixing appropriate



ionic sodium compounds **11a-c** with a solution of the appropriate N-alkyl-N-methylpiperidinium bromide **1h-m** in acetone. A minimum alkyl chain length of 14

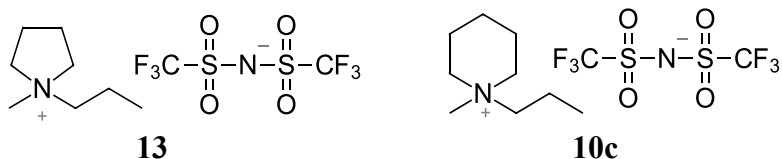
carbons atoms was necessary to induce mesomorphism. The cationic core and the anion type were shown to have a great influence on the mesomorphic behavior and only highly ordered crystalline smectic phases were observed.⁴

Micelle Formation by N-alkyl-N-methylpiperidinium bromide Ionic Liquids

N-alkyl-N-methylpiperidinium bromides **1j-l** were studied for their micellar behavior⁴ in aqueous solution in order to expand the understanding of piperidinium ionic liquid behavior. Also, the effect the alkyl chains have on ionic liquid phase behavior was compared for imidazolium and pyrrolidinium ionic liquids. The piperidinium bromides **1j-l** were characterized for micellar behavior by surface tension, electrical conductivity measurements and steady-state fluorescence measurements. The critical micelle concentration values were shown to decrease with increasing hydrocarbon chain length due to the enhanced hydrophobic interaction between the longer chains. The critical micelle concentration and thermodynamic parameters related to the formation of micelle were collected through an investigation of temperature effect on critical micelle concentration. The formation of micelles by **1j-l** was found to be as entropy-driven at low temperature (298K) and enthalpy-driven at high temperature (318K).⁵

Ionic liquid Electrolyte for Electrochemical Application

The ionic liquid N-methyl-N-propylpiperidinium bis(trifluoromethane-sulphonyl)imide **10c** has been studied as an electrolyte for usage in lithium ion electrochemical cells. Cells containing **10c** were compared to other cells containing N-methyl-N-propylpyridinium bis(trifluoromethane-sulphonyl)imide **13**.



It was determined that both of the ionic liquids **10c** and **13** could be used as an electrolyte in a lithium battery system. Ionic liquid **13** was shown to behave normally in the initial few charging-discharging cycles, but thereafter lost capacity. The charging-discharging cycle capacity for **10c** was very good except for the initial few charging-discharging cycles, which indicates the electrolyte was stable during later charge-discharge cycles. In general, the charging-discharging cycling behavior of the cell with **10c** as the electrolyte was better than that with **13**.⁶

The use of **10c** as a component of carbon-based double-layer capacitors was also studied. The conductivity of **10c** as a neat ionic liquid was measured at room temperature and was shown to be relatively low. It was concluded that the high viscosity of the ionic liquid was the reason for low conductivity. It was found that the conductivity could be increased by mixing the ionic liquid with a low viscosity solvent like acetonitrile. The stability of the electrolyte using the neat ionic liquid or its mixture with acetonitrile could be detected at the electrode and both showed relatively low stability.⁷ Double-layer capacitor performance was also studied by cyclic voltammetry and charging-discharging cycles. It was found that the capacity for the double-layer capacitors using **10c** showed similar characteristics as those of a lead-acid battery. However, the double-layer capacitor with **10c**/acetonitrile showed better cycling capability, so it would seem to be a good candidate for high-power energy storage equipment.⁷

Ionic liquids based on **10c** and **13** with the additive vinylene carbonate (**VC**) were synthesized and investigated for usage in rechargeable lithium ion batteries. The electrochemical performance was investigated by cyclic voltammetry, charge-discharge cycles and impedance spectroscopy. It was found that all the ionic liquids exhibit high

thermal stability and the decomposition temperatures were almost the same for the ionic liquids. When the temperature was at 25°, the cells containing the VC with ionic liquid electrolytes demonstrated good charge-discharge cycling stabilities.⁸

It was concluded that it would be much better to design an ionic liquid electrolyte that does not need additives to coat the electrodes for application in high voltage lithium ion batteries, in order to take advantage of the ionic liquids high stabilities properties.⁸

Phthalocyanine

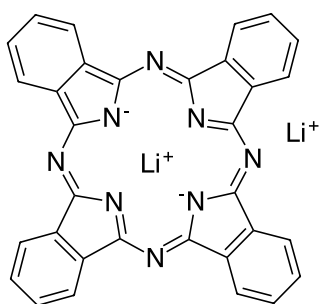
Phthalocyanine (Pc) was first synthesized in 1907.⁹ Subsequent studies revealed Pc potential as an exceptionally stable and insoluble pigment. During those studies, Pc was investigated by using elemental analysis, molecular mass determination and oxidative degradation to determine the structure for H₂Pc.¹⁰ It showed Pc as a symmetrical macrocycle composed of four iminoisoindoline units with a central cavity of sufficient size to accommodate various metal ions. The central cavity of Pc can hold seventy different ions ranging from hydrogen to americium. The metal cation will affect the physical properties of Pc. Some ions, like copper, are so tightly held in the cavity that removing them requires that the Pc ring be destroyed. Other cations, like lead, are too large to be accommodated completely in the cavity.¹¹ Alkali metal ions like lithium enhance the solubility of the Pc system in coordinating, polar organic solvents.¹²

Usage of Phthalocyanine

Pc and its derivatives were originally studied for use in the dye and pigment industry.¹³ Pcs have a limited range of color, from blue to green. The color is strongly dependent on the metal cation(s) used and/or the crystalline form of the Pc being studied.

The use of Pcs is not just limited to the dye and pigment industry. Pcs can be used in polymeric compositions with the ability to refine the properties.¹⁴ Pcs is also being used in thin film⁹, protective eyewear⁹ and optical data storage technology.⁹

Calculated Dilithium Phthalocyanine Structure



2

It was originally hypothesized¹⁵ that **2** would form an ionically conducting channel in which lithium ions could travel through the center of the phthalocyanine ring making **2** a potential lithium ion conductor that could be used in an all solid-state lithium ion battery. The structure of **2** was calculated using *ab initio* methods. The calculations predicted one lithium ion above and one below the open cavity in the plane of the Pc ring. Multiple molecules of **2** were employed in the calculations in order to predict interactions between the Pc rings. The calculations suggested staggered and shifted complexes being held together by electrostatic attraction between the lithium ions and nitrogen atoms in adjacent rings. One predicted pathway for the ionic conduction was a staircase configuration that would allow the lithium ions to flow through a continuous channel formed by the open cavity in the center of the Pc ring.¹⁶

Crystal Structure of Dilithium Phthalocyanine

The crystal structure of **2** was determined by single crystal x-ray diffraction. Crystals were obtained by recrystallization of **2** from an acetone/toluene solution over a

twelve-week period. The x-ray structure showed that one of the two lithium ions in **2** was coordinated in the center of the phthalocyanine ring but not perfectly centered in the ring plane. The lithium ion in the rings can either lie above the mean plane of the ring by 0.396Å or below it by 0.121Å. The second lithium ion was outside of the phthalocyanine ring and coordinated with water and acetone. Pairs of lithium phthalocyanine complex anions have a planar spacing of 3.38(2)Å and 3.062(2)Å. The pairs of phthalocyanine ligands were at a dihedral angle of 72.93(1)° to one another. The network was also held together by hydrogen bonds between the cations and anions.¹⁷

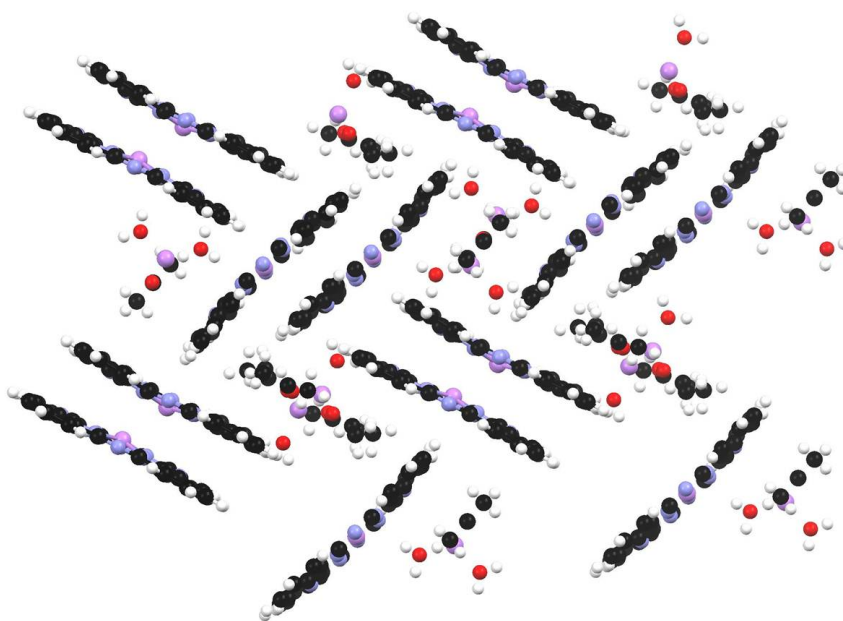
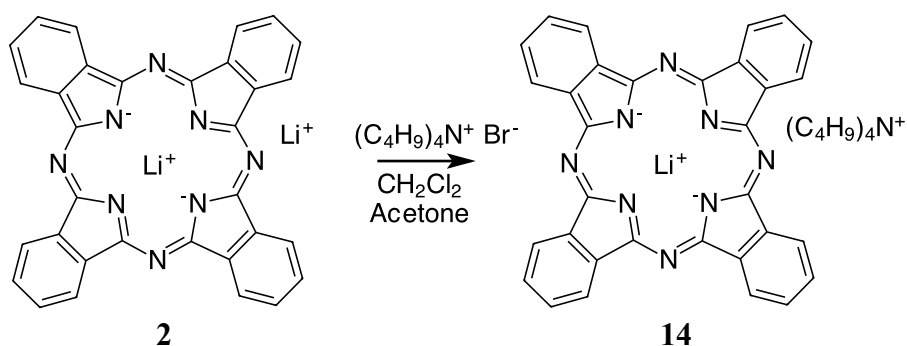


Figure 1. The crystal structure of **2** as obtained by single crystal x-ray diffraction.

The single crystal x-ray diffraction structure led to a reconsideration of the lithium ion conduction pathway through crystalline **2**. Lithium ions travel through the spacing, i.e. “channels” **between** the two phthalocyanine rings instead of through the cavity in the middle of the phthalocyanine rings.

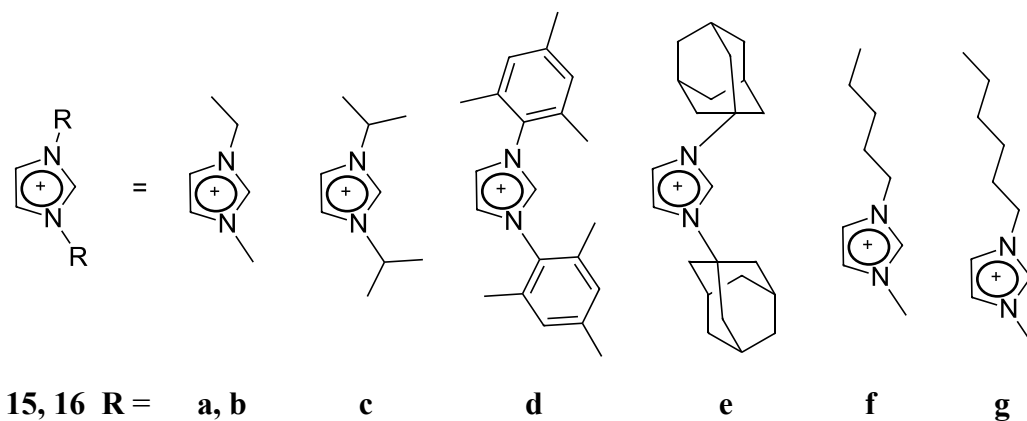
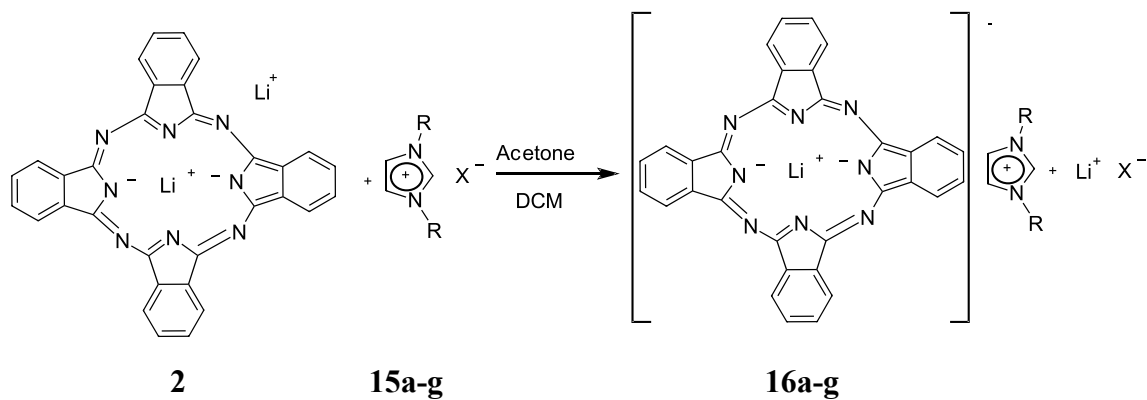
Exchange Reactions of Dilithium Phthalocyanine

The first example of an exchange reaction between the “mobile” lithium ion in **2** and a tetraalkylammonium halide **20d** was reported by Homberg.^{18, 19} Thus, **2** was reacted with tetrabutylammonium bromide **20d** in a mixture of DCM and acetone. The product,



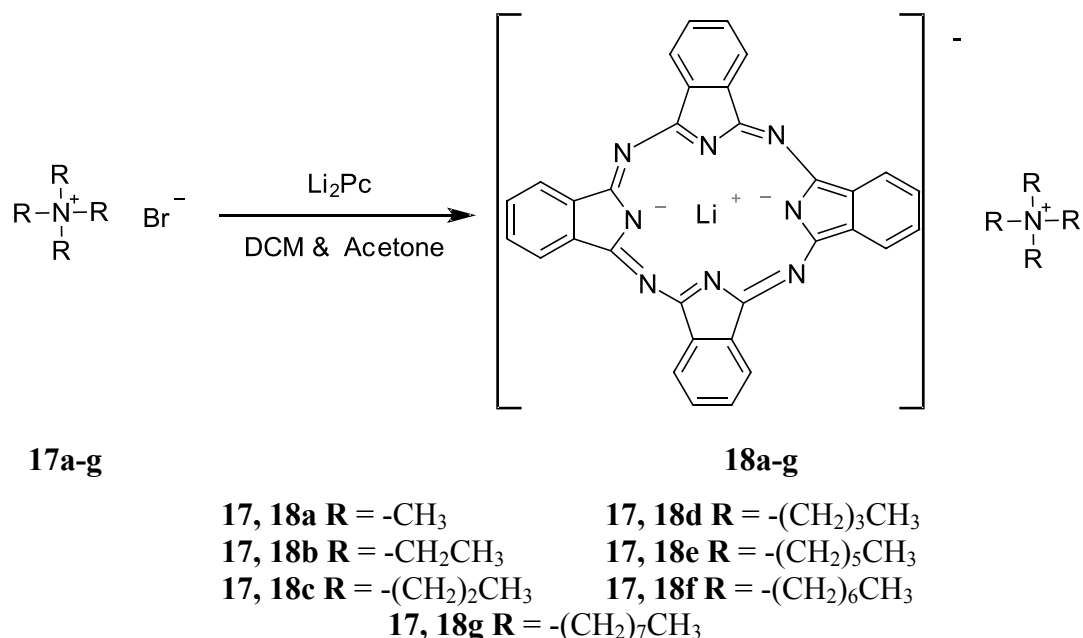
tetrabutylammonium lithium phthalocyanine **14**, was isolated as a purple solid in an undisclosed yield. Later, the crystal structure of **14** was determined and revealed a lithium phthalocyanine complex anion separation of about 7 Å. This can be compared to the interring spacing of about 3.5 Å in dilithium phthalocyanine.²⁰

A series of imidazolium lithium phthalocyanine compounds for possible use in lithium ion technologies was synthesized in 2008.²¹ The synthesis was carried out using dilithium phthalocyanine **2** with 1-ethyl-3-methylimidazolium chloride **15a**, 1-ethyl-3-methylimidazolium bis(pentafluoroethylsulfonyl)imide **15b**, 1,3-diisopropylimidazolium tetrafluoroborate **15c**, 1,3-bis(2,4,6-trimethylphenyl)imidazolium chloride **15d**, 1,3-bis(1-adamantyl)imidazolium tetrafluoroborate **15e**, 1-pentyl-3-methylimidazolium bis(pentafluoroethylsulfonyl)imide **15f** or 1-hexyl-3-methylimidazolium chloride **15g**. The reactions were carried out either in the presence of acetone or dichloromethane.



The exchange products **16a-g** were obtained in yields from 9-81% and were characterized by ^1H and ^{13}C NMR, IR, elemental analysis, TGA and single-crystal XRD. The exchange products were observed having unique C-C and C-N stretching modes in their IR spectra that are characteristic for phthalocyanine and imidazolium aromatic rings. The TGA showed all the exchange products were thermally stable up to at least 300° .

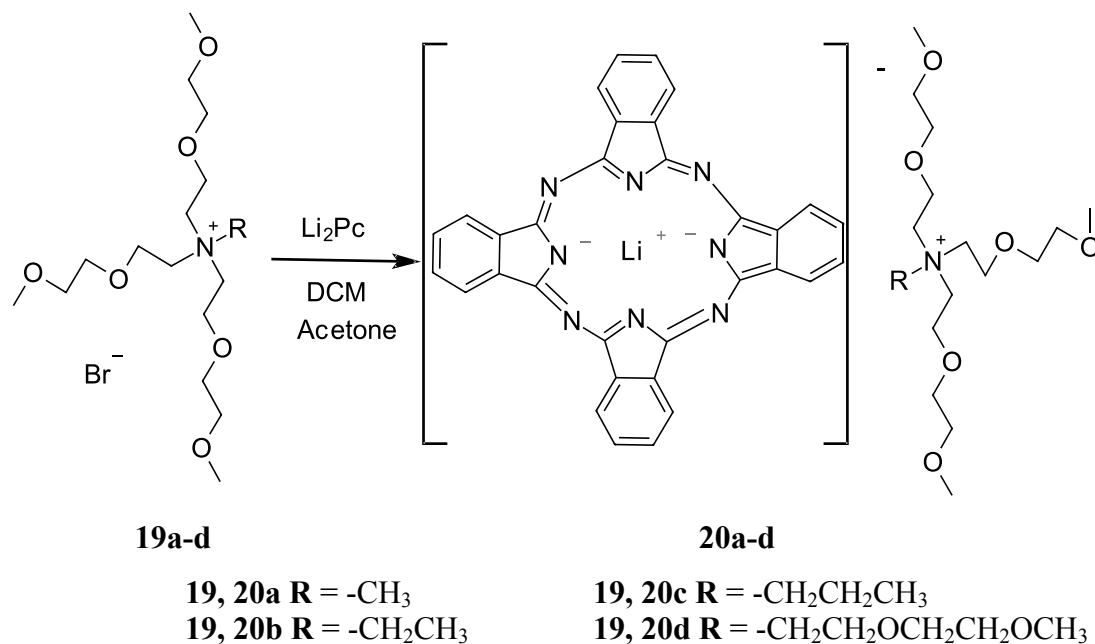
An extension²² of Homberg's initial exchange reaction involved the reaction of **2** in acetone solution with tetramethylammonium **17a**, tetraethylammonium **17b**, tetrapropylammonium **17c**, tetrabutylammonium **17d**, tetrahexylammonium **17e**, tetraheptylammonium **17f** and tetraoctylammonium **17g** in dichloromethane.



The exchange products **18a-g** were characterized by melting points, IR, ¹H and ¹³C NMR spectra, and powder XRD. Melting points decreased as the alkyl chain length of the ammonium cations increased. One interesting feature of this series is the observation that ¹H NMR spectra for the exchange products in CDCl₃ exhibit alkyl chain chemical shifts that are shifted far upfield compared to those observed in samples run in acetone-d₆. The upfield shift was proposed to be the effect of shielding due to an interaction between the cation and anion. Powder XRD spectra showed that compounds **18a** and **18g** had far less peaks in the diffraction pattern than the other compounds **18b-f**, indicating that they have a less crystalline structure. The yields for the exchange series ranged from 54 – 64%.

A unique exchange series was generated by reacting **2** with the alkoxyalkylammonium salts, tris((2-methoxyethoxy)ethoxy)methylammonium bromide **19a**, tris((2-methoxyethoxy)ethoxy)ethylammonium bromide **19b**, tris((2-methoxyethoxy)ethoxy)propylammonium bromide **19c** and tetra(2-

methoxyethoxy)ethoxyammonium bromide **19d**. The reactions were conducted in acetone or acetone/DCM mixtures and the exchange products **20a-d** were isolated in yields ranging from 43-73%.



Exchange products **20a-d** were characterized by melting point, ¹H and ¹³C NMR spectra, IR, thermal analysis, and single crystal x-ray analysis. A majority of the exchange products were thermally stable to 300°, excepted for **20a** which was only stable to 250°. The melting points ranged from 118-160°. Single crystal x-ray diffraction studies for compounds **20a-d** were examined. The ring spacing of the lithium phthalocyanine complex anions was 3.38Å and can be compared to the spacing of the rings of 14.07Å in **20c** and 10.5Å in **20d**. The exact location of the atoms of the alkoxyalkyl chains in the cations is not possible due to a high disorder factor for those atoms.²³

In view of the considerable effort expended in the synthesis of piperidinium-based ionic liquids and nitrogen-based quaternary ammonium lithium phthalocyanine complexes, the objectives of this research were to 1) develop an efficient solvent free

method of synthesizing N-alkyl-N-methylpiperidinium halides, 2) characterize the halides by melting point, NMR, IR, and elemental analysis and 3) use selected piperidinium halides in an exchange reaction with dilithium phthalocyanine.

Experimental

Melting points were obtained with DigiMelt MPA-160. Nuclear magnetic Resonance (NMR) ^1H , ^{13}C , and ^{13}C Dept135 spectra were obtained using a Bruker Avance 300 MHz Spectrometer. The solvents for NMR were CDCl_3 , DMSO-d_6 and Acetone- d_6 . Infrared (IR) spectra were recorded as thin films (NaCl plate) with a Nicolet 6700 FT-IR. Thermal Gravimetric Analysis (TGA) and Differential Scanning Calorimetry (DSC) spectra were obtained with the instruments TA TGA Q 500 and TA DSC Q 200 both employing N_2 atmosphere and TGA also employing O_2 atmosphere. Elemental analyses were obtained through Midwest Microlab, LLC, Indianapolis, IN. A 35mL Q-TubeTM (pressure tube reactor) was used for reactions involving volatile materials. Starting materials were purchased from Aldrich and used as received.

General Procedure for the Reaction of N-methylpiperidine and 1-bromoalkanes.

A solution of N-methylpiperidine and the appropriate 1-bromoalkane (1:1.5 molar ratio) was placed in a Q-TubeTM and heated at 100° for 24 h with stirring. After cooling, the solid product was washed three times with ethyl acetate, air dried and finally vacuum dried for 18 h at 50° .

N-Methyl-N-propylpiperidinium Bromide (PIP₁₃Br) 1c.

A white solid was obtained in 71% yield: m.p. $249.9 - 250.9^\circ\text{C}$, ^1H NMR (300MHz, CDCl_3) δ 3.68 (m, 6H, $-\text{CH}_2$), 3.35 (s, 3H, $-\text{CH}_3$), 1.89 (m, 8H, $-\text{CH}_2$), 1.03 (t, 3H, $-\text{CH}_3$); ^{13}C NMR (75 MHz, CDCl_3) δ 64.61, 60.93, 48.33, 20.70, 20.21, 15.56, 10.84;

^{13}C Dept135 NMR (75 MHz, CDCl_3) δ $-\text{CH}_3$: 48.32, 10.85, $-\text{CH}_2$: 64.59, 60.92, 20.70, 20.21, 15.55; IR (NaCl salt plate) cm^{-1} 2954 (C-H), 1468 (C-H). Anal. Calc. for $\text{C}_9\text{H}_{20}\text{BrN}$ (222.16): C, 48.66; H, 9.07; N, 6.30. Found: C, 48.86; H, 8.91; N, 6.37.

N-Methyl-N-butylpiperidinium Bromide (PIP₁₄Br) 1d.

A white solid was obtained in 89% yield: m.p. 239.1 – 240.5°C, ^1H NMR (300MHz, CDCl_3) δ 3.72 (m, 6H, $-\text{CH}_2$), 3.32 (s, 3H, $-\text{CH}_3$), 1.82 (m, 8H, $-\text{CH}_2$), 1.49 (m, 2H, $-\text{CH}_2$), 1.02 (t, 3H, $-\text{CH}_3$); ^{13}C NMR (75 MHz, CDCl_3) δ 62.97, 60.86, 48.25, 23.89, 20.67, 20.21, 19.71, 13.72; ^{13}C Dept135 NMR (75 MHz, CDCl_3) δ $-\text{CH}_3$: 48.25, 13.73, $-\text{CH}_2$: 62.96, 60.85, 23.89, 20.67, 20.20, 19.71, 13.73; IR (NaCl salt plate) cm^{-1} 2940 (C-H), 1466 (C-H); Anal. Calc. for $\text{C}_{10}\text{H}_{22}\text{BrN}$ (236.19): C, 50.85; H, 9.39; N, 5.93. Found: C, 50.91; H, 9.36; N, 5.88.

N-Methyl-N-pentylpiperidinium Bromide (PIP₁₅Br) 1e.

A white solid was obtained in 89% yield: m.p. 192.4 – 195.5°C, ^1H NMR (300MHz, CDCl_3) δ 3.73 (m, 6H, $-\text{CH}_2$), 3.33 (s, 3H, $-\text{CH}_3$), 1.85 (m, 8H, $-\text{CH}_2$), 1.42 (m, 4H, $-\text{CH}_2$), 0.94 (t, 3H, $-\text{CH}_3$); ^{13}C NMR (75 MHz, CDCl_3) δ 63.08, 60.85, 48.31, 28.38, 22.29, 21.70, 20.68, 20.22, 13.80; ^{13}C Dept135 NMR (75 MHz, CDCl_3) δ $-\text{CH}_3$: 48.32, 13.81, $-\text{CH}_2$: 63.05, 60.83, 28.37, 22.30, 21.70, 20.68, 20.22; IR (NaCl salt plate) cm^{-1} 2953 (C-H), 1470 (C-H); Anal. Calc. for $\text{C}_{11}\text{H}_{24}\text{BrN}$ (250.21): C, 52.80; H, 9.67; N, 5.60. Found: C, 52.82; H, 9.59; N, 5.63.

N-Methyl-N-hexylpiperidinium Bromide (PIP₁₆Br) 1f.

A white solid was obtained in 87% yield: m.p. 192.8 – 196.0°C, ^1H NMR (300MHz, CDCl_3) δ 3.68 (m, 6H, $-\text{CH}_2$), 3.32 (s, 3H, $-\text{CH}_3$), 1.85 (m, 8H, $-\text{CH}_2$), 1.34 (m, 6H, $-\text{CH}_2$), 0.87 (t, 3H, $-\text{CH}_3$); ^{13}C MR (75 MHz, CDCl_3) δ 63.14, 60.83, 48.26,

31.25, 25.98, 22.33, 21.95, 20.64, 20.19, 13.83; ^{13}C Dept135 NMR (75 MHz, CDCl_3) δ –
 CH_3 : 48.26, 13.84, $-\text{CH}_2$: 63.12, 60.82, 31.26, 25.98, 22.34, 21.95, 20.64, 20.19; IR
(NaCl salt plate) cm^{-1} 2936 (C-H), 1469 (C-H); Anal. Calc. for $\text{C}_{12}\text{H}_{26}\text{BrN}$ (264.24): C,
54.54; H, 9.92; N, 5.30. Found: C, 53.68; H, 9.79; N, 5.53.

N-Methyl-N-heptylpiperidinium Bromide (PIP₁₇Br) 1g.

A white solid was obtained in 85% yield: m.p. 190.6 – 194.5°C, ^1H NMR
(300MHz, CDCl_3) δ 3.67 (m, 6H, $-\text{CH}_2$), 3.32 (s, 3H, $-\text{CH}_3$), 1.70 (m, 8H, $-\text{CH}_2$), 1.31
(m, 8H, $-\text{CH}_2$), 0.85 (t, 3H, $-\text{CH}_3$); ^{13}C NMR (75 MHz, CDCl_3) δ 63.05, 60.83, 48.35,
31.49, 28.86, 26.32, 22.41, 22.03, 20.67, 20.22, 13.96; ^{13}C Dept135 NMR (75 MHz,
 CDCl_3) δ $-\text{CH}_3$: 48.35, 13.97, $-\text{CH}_2$: 63.05, 60.83, 31.49, 28.87, 26.32, 22.42, 22.03,
20.66, 20.21; IR (NaCl salt plate) cm^{-1} 2928 (C-H), 1469 (C-H); Anal. Calc. for
 $\text{C}_{13}\text{H}_{28}\text{BrN}$ (278.27): C, 56.11; H, 10.14; N, 5.03. Found: C, 56.17; H, 9.87; N, 5.03.

General Procedure for the preparation of N-alkyl-N-methylpiperidinium lithium phthalocyanines.

A solution of dilithium phthalocyanine 5 mmol in acetone was filtered. The filtrate of the dilithium phthalocyanine solution was added dropwise to a solution of the appropriate N-alkyl-N-methylpiperidinium bromide 2 mmol in dichloromethane with stirring. The precipitate was collected, washed with acetone, air dried and finally vacuum dried for 18 hr. at 50°C.

N-Methyl-N-propylpiperidinium lithium phthalocyanine 21.

A purple powder was obtained in 78% yield: ^1H NMR (300MHz, DMSO-d_6) δ
9.32 (q, 8H, Aro-H), 8.06 (q, 8H, Aro-H), 3.03 (m, 6H, $-\text{CH}_2$), 2.75 (s, 3H, $-\text{CH}_3$), 1.48

(m, 8H, -CH₂), 0.78 (t, 3H, -CH₃); Anal. Calc. for C₄₁H₃₆LiN₉ (661.33): C, 74.42; H, 5.48; N, 19.05. Found: C, 74.49; N, 19.04; H, 5.41.

N-Methyl-N-butylpiperidinium lithium phthalocyanine 22.

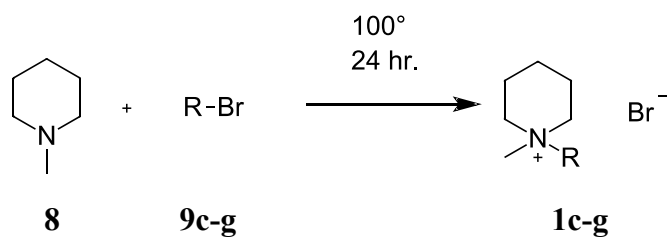
A blue solid was obtained in 85% yield: ¹H NMR (300MHz, DMSO-d₆) δ 9.32 (q, 8H, Aro-H), 8.06 (q, 8H, Aro-H), 3.12 (m, 6H, -CH₂), 2.83 (s, 3H, -CH₃), 1.54 (m, 8H, -CH₂), 1.23 (m, 2H, -CH₂), 0.87 (t, 3H, -CH₃); Anal. Calc. for C₄₂H₃₈LiN₉ (675.34): C, 74.65; H, 5.67; N, 18.65. Found: C, 74.35; N, 18.65; H, 5.47.

RESULTS AND DISCUSSION

A series of N-alkyl-N-methylpiperidinium bromides **1c-g** were synthesized by a simple nucleophilic substitution. The reactions used N-methylpiperidine **8** with a range of bromoalkanes **9c-g** to produce N-alkyl-N-methylpiperidinium bromides **1c-g**, by a solvent free method. A Q-Tube™ was used to facilitate the use of low boiling bromoalkanes and to allow an elevated temperature to be used for the reaction. The Q-Tube™ method allows the reaction to be solvent free. The salts were purified by an ethyl acetate wash.

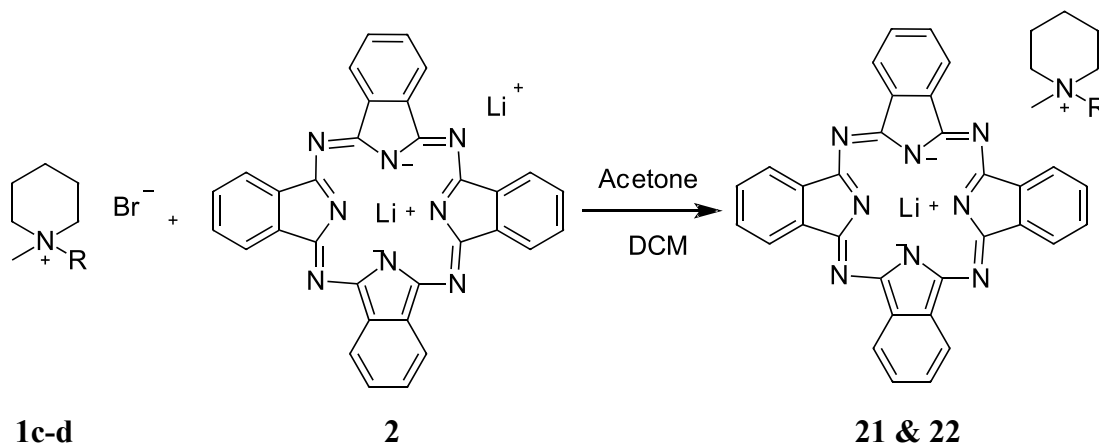


Image 1: Q-Tube™ setup.



Two of the salts, **1c** and **1d** were used in the exchange reaction with **2** to synthesize a series of N-alkyl-N-methylpiperidinium lithium phthalocyanines **21** and **22**.

The extraneous ions (e.g. LiBr) were removed by the acetone wash to provide compounds **21** and **22**.



The abbreviations for all the compounds being discussed will be referred to the list in **Table 1**.

Table 1. Compounds numbers and abbreviation that been research.

Number	Compound	Abbreviation
1c	N-methyl-N-propylpiperidinium bromide	PIP ₁₃ Br
1d	N-methyl-N-butylpiperidinium bromide	PIP ₁₄ Br
1e	N-methyl-N-pentylpiperidinium bromide	PIP ₁₅ Br
1f	N-methyl-N-hexylpiperidinium bromide	PIP ₁₆ Br
1g	N-methyl-N-heptylpiperidinium bromide	PIP ₁₇ Br
21	N-methyl-N-propylpiperidinium lithium phthalocyanine	PIP ₁₃ LiPc
22	N-methyl-N-butylpiperidinium lithium phthalocyanine	PIP ₁₄ LiPc

Elemental Analysis

Elemental analysis was performed on all compounds synthesized. The elemental analysis established the elemental composition of all samples. The carbon, hydrogen and nitrogen analyses for the samples were in good agreement with the calculated values.

Table 2. Elemental Analysis Results.

Compound (#)	Calc'd	Found	Compound (#)	Calc'd	Found
PIP ₁₃ Br (1c)	C: 48.66	C: 48.86	PIP ₁₄ Br (1d)	C: 50.85	C: 50.91
	H: 9.07	H: 8.91		H: 9.39	H: 9.36
	N: 6.30	N: 6.37		N: 5.93	N: 5.88
PIP ₁₅ Br (1e)	C: 52.80	C: 52.82	PIP ₁₆ Br (1f)	C: 54.54	C: 53.68
	H: 9.67	H: 9.59		H: 9.92	H: 9.79
	N: 5.60	N: 5.63		N: 5.30	N: 5.53
PIP ₁₇ Br (1g)	C: 56.11	C: 56.17	PIP ₁₃ LiPc 21	C: 74.42	C: 74.49
	H: 10.14	H: 9.87		H: 5.48	H: 5.41
	N: 5.03	N: 5.03		N: 19.05	N: 19.04
PIP ₁₄ LiPc 22	C: 74.65	C: 74.35			
	H: 5.67	H: 5.47			
	N: 18.65	N: 18.65			

Melting point

The melting points of the N-methyl-N-alkylpiperidinium bromides **1c-g** show a decrease in melting point temperature as the alkyl chain length increase. There is a slight plateau in the melting point temperature from **1e** to **1f**, where the melting points are very close together. The exchange reaction products had melting points above the capillary instrument range (>363.3°C).

Table 3. Melting point results.

Compound (#)	Melting point (°C)
PIP ₁₃ Br (1c)	249.9 - 250.9 °C
PIP ₁₄ Br (1d)	239.1 - 240.5 °C
PIP ₁₅ Br (1e)	192.4 - 195.5 °C
PIP ₁₆ Br (1f)	192.8 - 195.9 °C
PIP ₁₇ Br (1g)	190.6 - 194.5 °C

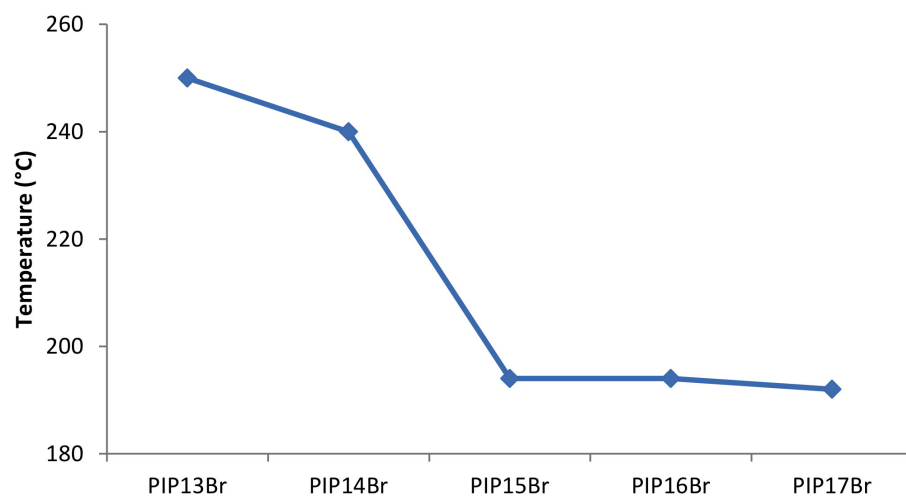


Figure 2. Melting points results.

¹H NMR Spectroscopy

The ¹H NMR Spectra for the **8** and PIP1_nBr **1c-g** were performed in CDCl₃, while the exchange products **21** and **22** were performed in DMSO-d₆. The exchange products would not dissolved in CDCl₃.

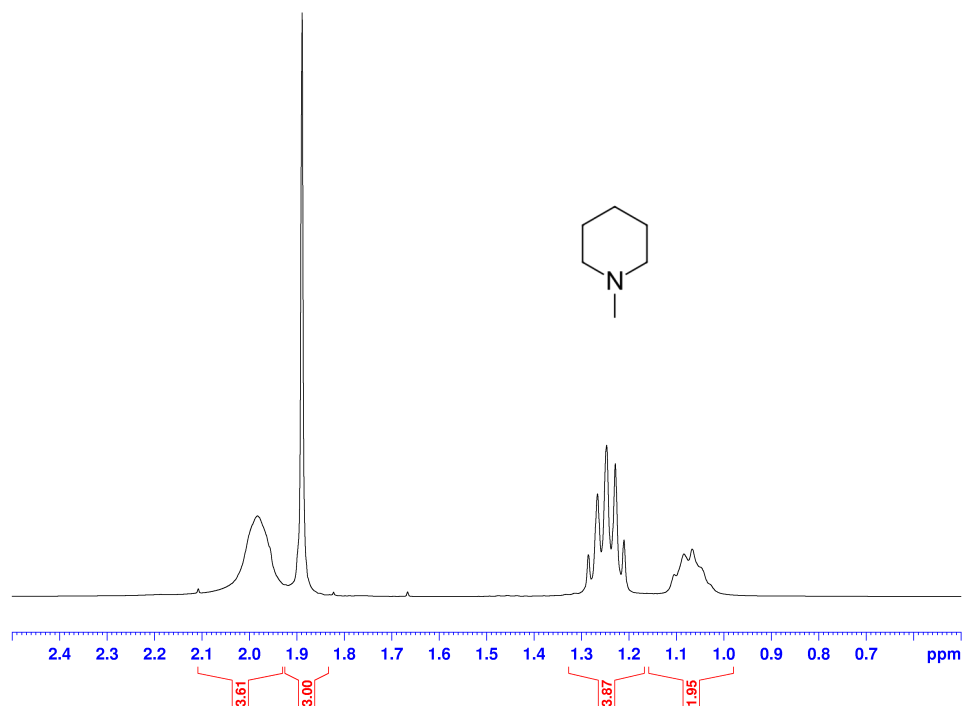


Figure 3. ¹H NMR spectrum (CDCl₃) of N-methylpiperidine **8**.

The ^1H NMR spectrum of N-methylpiperidine **8** exhibited a multiplet absorption at 1.09 δ that can be attributed to the protons (d) of the CH_2 that is opposite from the nitrogen. The quintet absorption at 1.25 δ can be attributed to the two CH_2 groups (c) that are beta from the nitrogen atom. The singlet absorption at 1.89 δ can be attributed to the CH_3 (a) that is attached to the nitrogen atom. The singlet absorption at 1.99 δ can be attributed to the two CH_2 groups (b) that are attached the nitrogen.

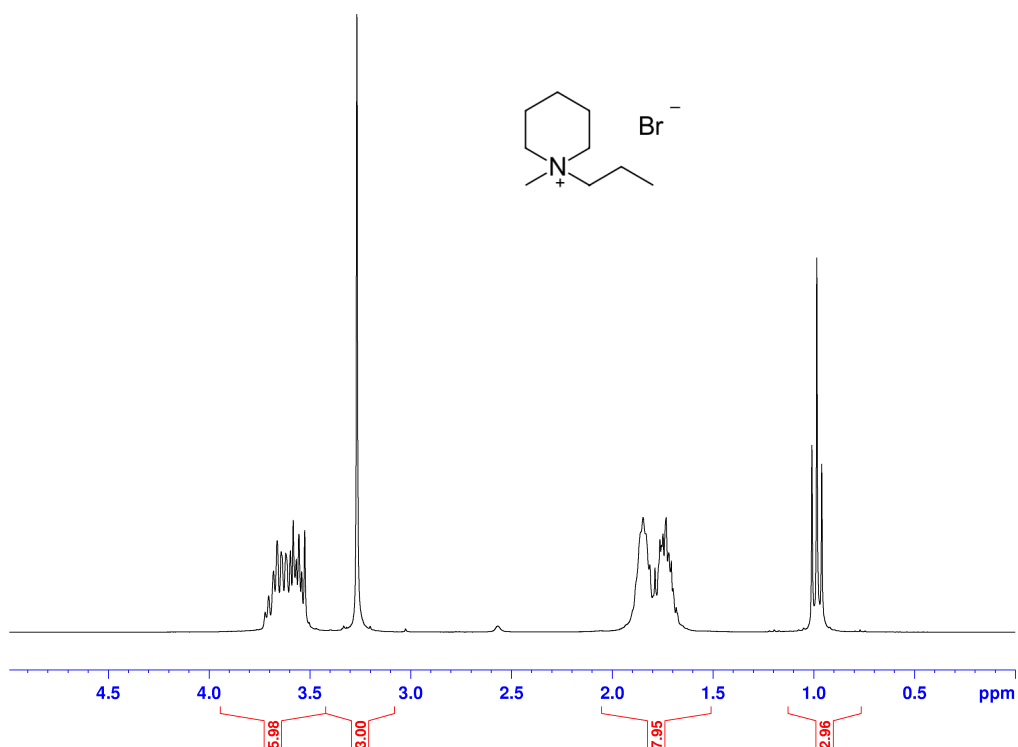


Figure 4. ^1H NMR spectrum (CDCl_3) of PIP₁₃Br **1c**.

The ^1H NMR spectrum of PIP₁₃Br **1c** exhibited a triplet absorption at 1.03 δ that can be attributed to the protons (a) of the CH_3 on the propyl group. The multiplet absorption at 1.89 δ can be attributed to the three CH_2 groups (b) that are on the beta carbon from the nitrogen atom and the CH_2 group (b) that is opposite from the nitrogen in the ring. The singlet absorption at 3.35 δ can be attributed to the CH_3 (d) that is attached

to the nitrogen atom. The multiplet absorption at 3.68 δ can be attributed to the three CH_2 groups (c) that are attached to the nitrogen.

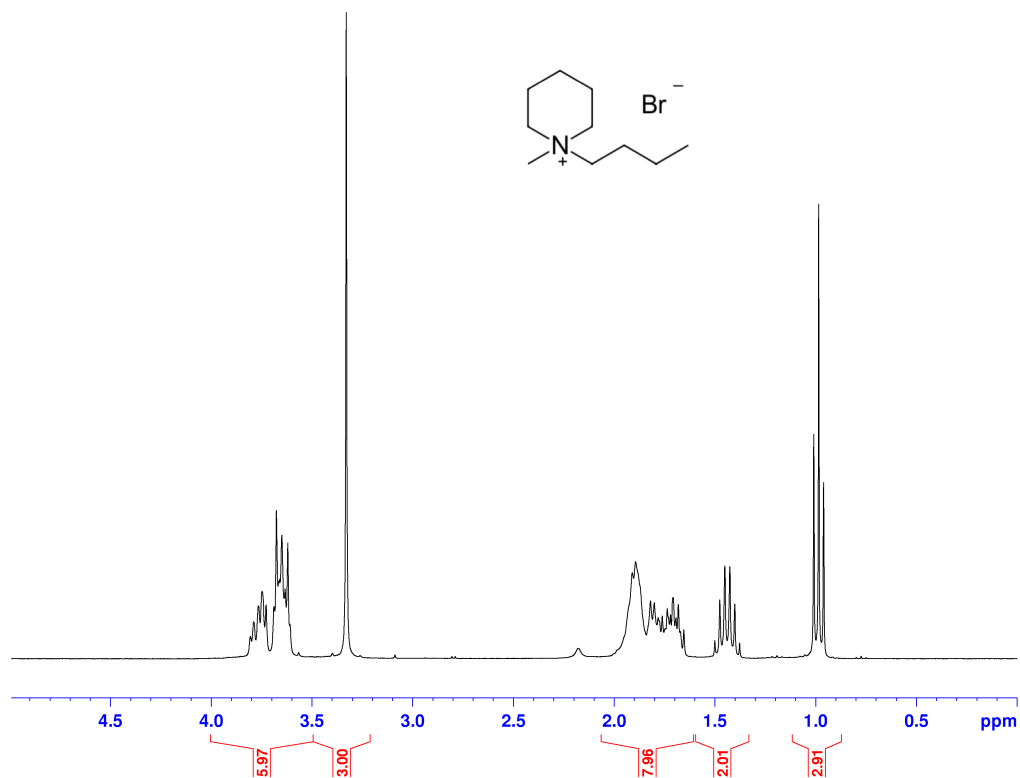


Figure 5. ^1H NMR spectrum (CDCl_3) of PIP_{14}Br **1d**.

The ^1H NMR spectrum of PIP_{14}Br **1d** exhibited a triplet absorption at 1.02 δ that can be attributed to the protons (a) of the CH_3 on the butyl group. The sextet absorption at 1.49 δ can be attributed to the CH_2 group (b) next to the CH_3 on the butyl group. The multiplet absorption at 1.82 δ can be attributed to the three CH_2 groups (c) that are on the beta carbon from the nitrogen atom and the CH_2 group (c) that is opposite from the nitrogen in the ring. The singlet absorption at 3.32 δ can be attributed to the CH_3 (e) that is attached to the nitrogen atom. The multiplet absorption at 3.72 δ can be attributed to the three CH_2 groups (d) that are attached to the nitrogen.

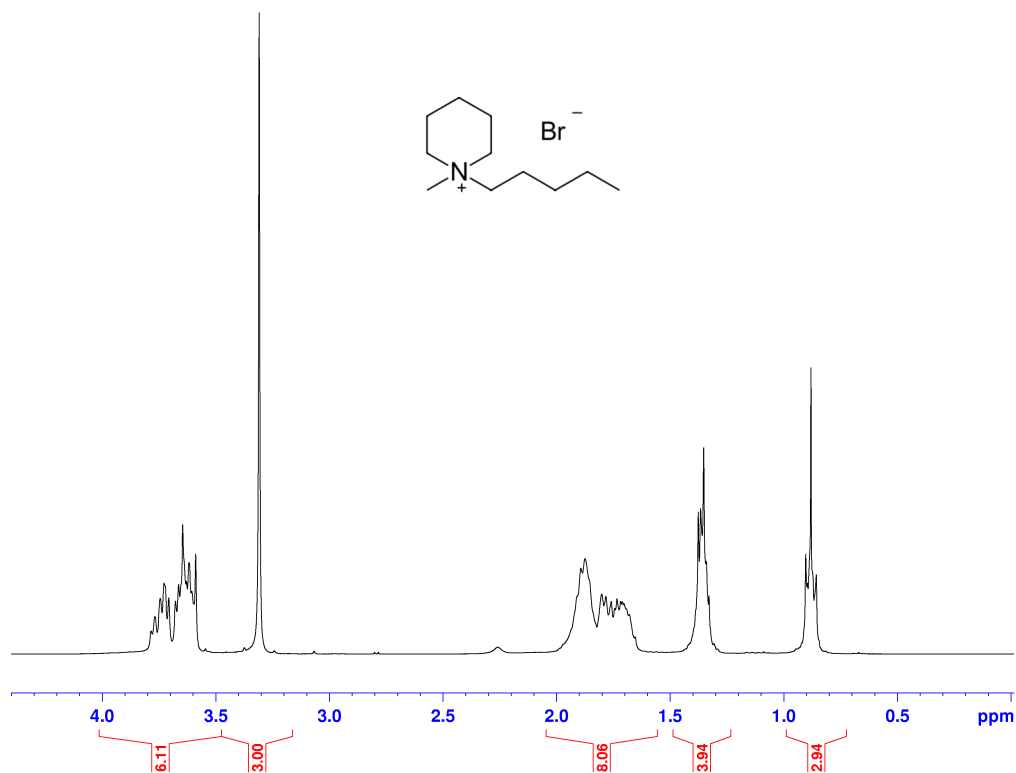


Figure 6. ^1H NMR spectrum (CDCl_3) of PIP_{15}Br **1e**.

The ^1H NMR spectrum of PIP_{15}Br **1e** exhibited a triplet absorption at 0.94 δ that can be attributed to the protons (a) of the CH_3 on the pentyl group. The multiplet absorption at 1.42 δ can be attributed to the two CH_2 groups (b) closest to the CH_3 on the pentyl group. The multiplet absorption at 1.85 δ can be attributed to the three CH_2 groups (c) that are on the beta carbon from the nitrogen atom and the CH_2 group (c) that is opposite from the nitrogen in the ring. The singlet absorption at 3.33 δ can be attributed to the CH_3 (e) that is attached to the nitrogen atom. The multiplet absorption at 3.73 δ can be attributed to the three CH_2 groups (d) that are attached to the nitrogen.

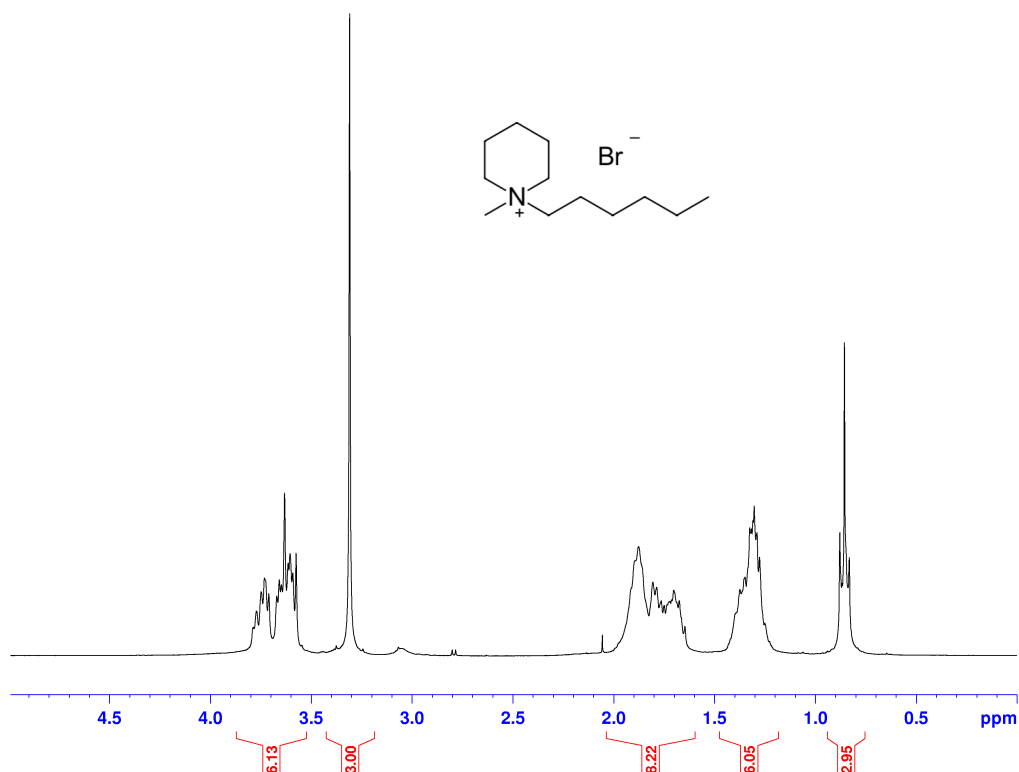


Figure 7. ^1H NMR spectrum (CDCl_3) of PIP_{16}Br **1f**.

The ^1H NMR spectrum of PIP_{16}Br **1f** exhibited a triplet absorption at $0.87\ \delta$ that can be attributed to the protons (a) of the CH_3 on the hexyl group. The multiplet absorption at $1.34\ \delta$ can be attributed to the three CH_2 groups (b) closest to the CH_3 on the hexyl group. The multiplet absorption at $1.85\ \delta$ can be attributed to the three CH_2 groups (c) that are on the beta carbon from the nitrogen atom and the CH_2 group (c) that is opposite from the nitrogen in the ring. The singlet absorption at $3.32\ \delta$ can be attributed to the CH_3 (e) that is attached to the nitrogen atom. The multiplet absorption at $3.68\ \delta$ can be attributed to the three CH_2 groups (d) that are attached to the nitrogen.

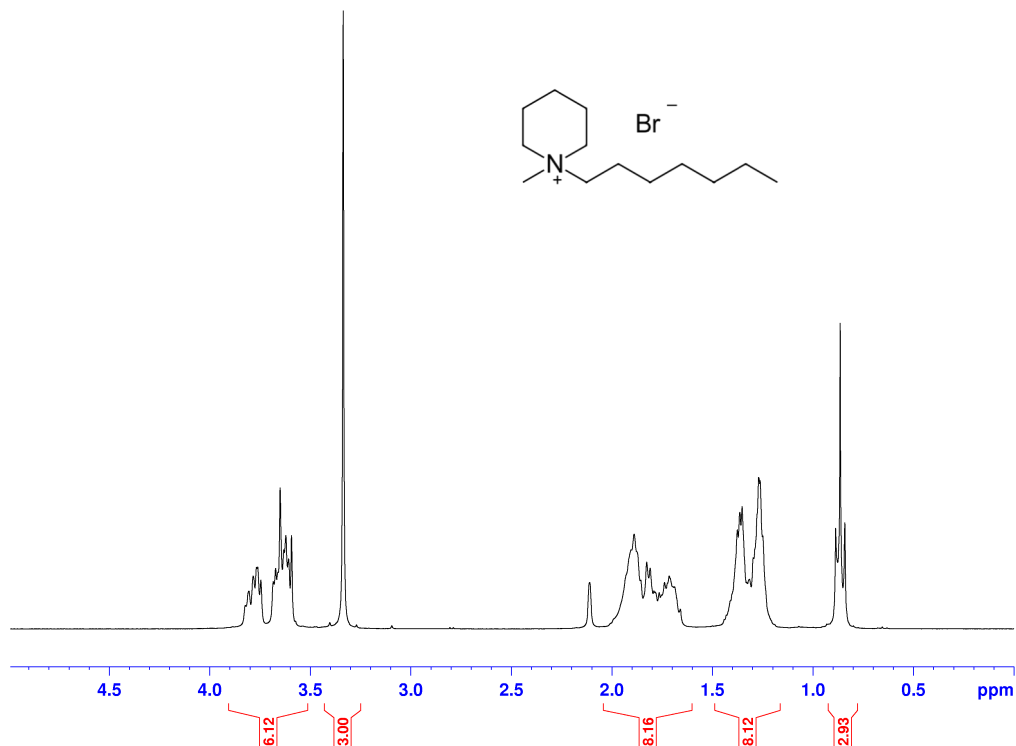


Figure 8. ^1H NMR spectrum (CDCl_3) of PIP_{17}Br **1g**.

The ^1H NMR spectrum of PIP_{17}Br **1g** exhibited a triplet absorption at $0.85\ \delta$ that can be attributed to the protons (a) of the CH_3 on the heptyl group. The multiplet absorption at $1.31\ \delta$ can be attributed to the four CH_2 groups (b) closest to the CH_3 on the heptyl group. The multiplet absorption at $1.70\ \delta$ can be attributed to the three CH_2 groups (c) that are on the beta carbon from the nitrogen atom and the CH_2 group (c) that is opposite from the nitrogen in the ring. The singlet absorption at $3.32\ \delta$ can be attributed to the CH_3 (e) that is attached to the nitrogen atom. The multiplet absorption at $3.67\ \delta$ can be attributed to the three CH_2 groups (d) that are attached to the nitrogen.

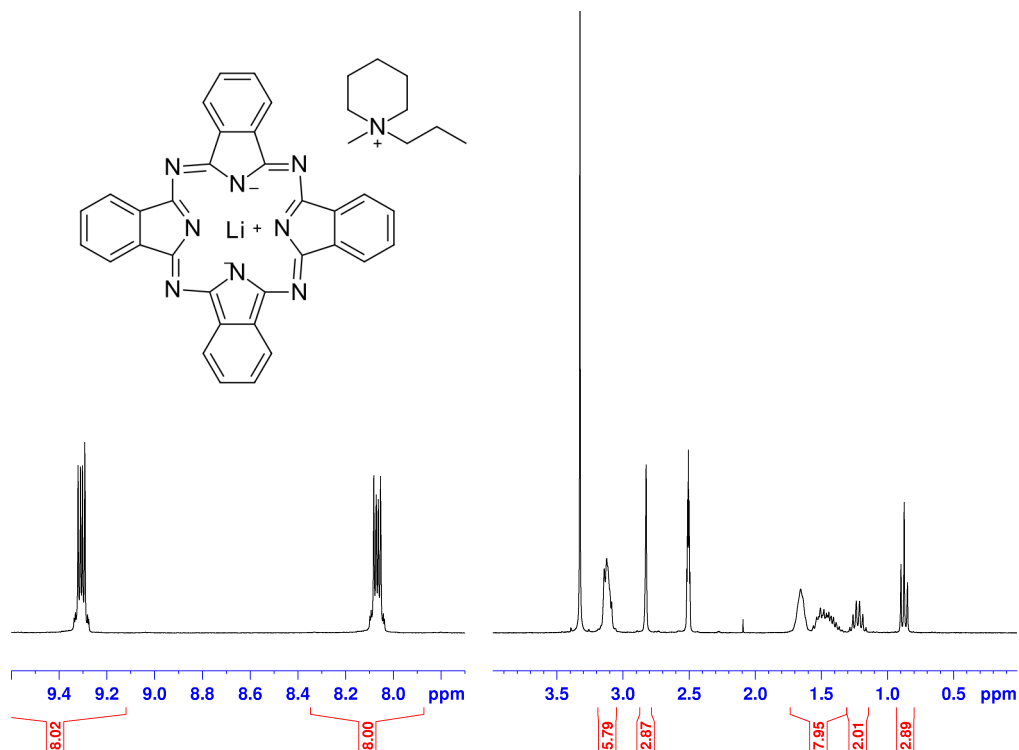


Figure 9. ^1H NMR spectrum (DMSO- d_6) of PIP $_{13}$ Br LiPc **21**.

The ^1H NMR spectrum of PIP $_{13}$ Br LiPc **21** exhibited a triplet absorption at 1.03 δ that can be attributed to the protons (a) of the CH_3 on the propyl group. The multiplet absorption at 1.89 δ can be attributed to the three CH_2 groups (b) that are on the beta carbon from the nitrogen atom and the CH_2 group (b) that is opposite from the nitrogen in the ring. The singlet absorption at 3.35 δ can be attributed to the CH_3 (d) that is attached to the nitrogen atom. The multiplet absorption at 3.68 δ can be attributed to the three CH_2 groups (c) that are attached to the nitrogen.

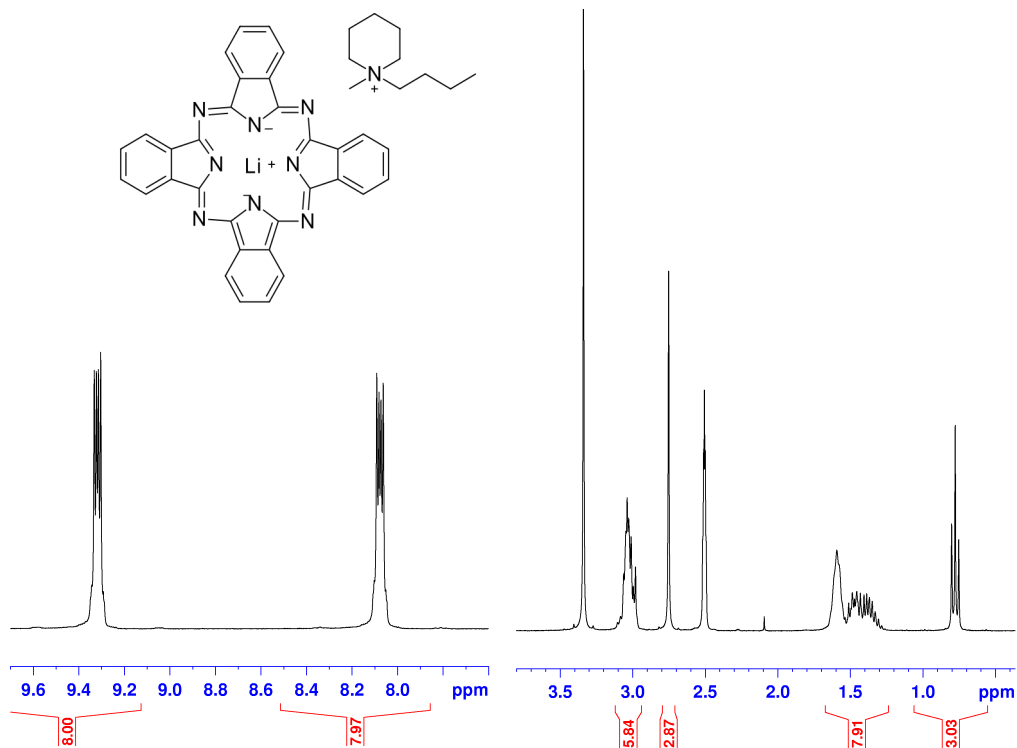


Figure 10. ^1H NMR spectrum (DMSO- d_6) of PIP $_{14}$ Br LiPc **22**.

The ^1H NMR spectrum of PIP $_{14}$ Br LiPc **22** exhibited a triplet absorption at 0.87 δ that can be attributed to the protons (a) of the CH_3 on the butyl group. The sextet absorption at 1.23 δ can be attributed to the CH_2 group (b) next to the CH_3 on the butyl group. The multiplet absorption at 1.54 δ can be attributed to the three CH_2 groups (c) that are on the beta carbon from the nitrogen atom and the CH_2 group (c) that is opposite from the nitrogen in the ring. The singlet absorption at 2.83 δ can be attributed to the CH_3 (e) that is attached to the nitrogen atom. The multiplet absorption at 3.12 δ can be attributed to the three CH_2 groups (d) that are attached to the nitrogen. The two quartet absorptions at 8.06 δ and 9.32 δ can be attributed to the anion aromatic rings at the (g) and (f) position, respectively.

¹³C and Dept 135 NMR Spectroscopy

The ¹³C and Dept 135 NMR Spectra for the **8** and PIP1_nBr **1c-g** were performed in CDCl₃. The exchange products were not done because the samples were only slightly soluble in DMSO-d₆. So the concentrations of the samples were not high enough to obtain clean spectra.

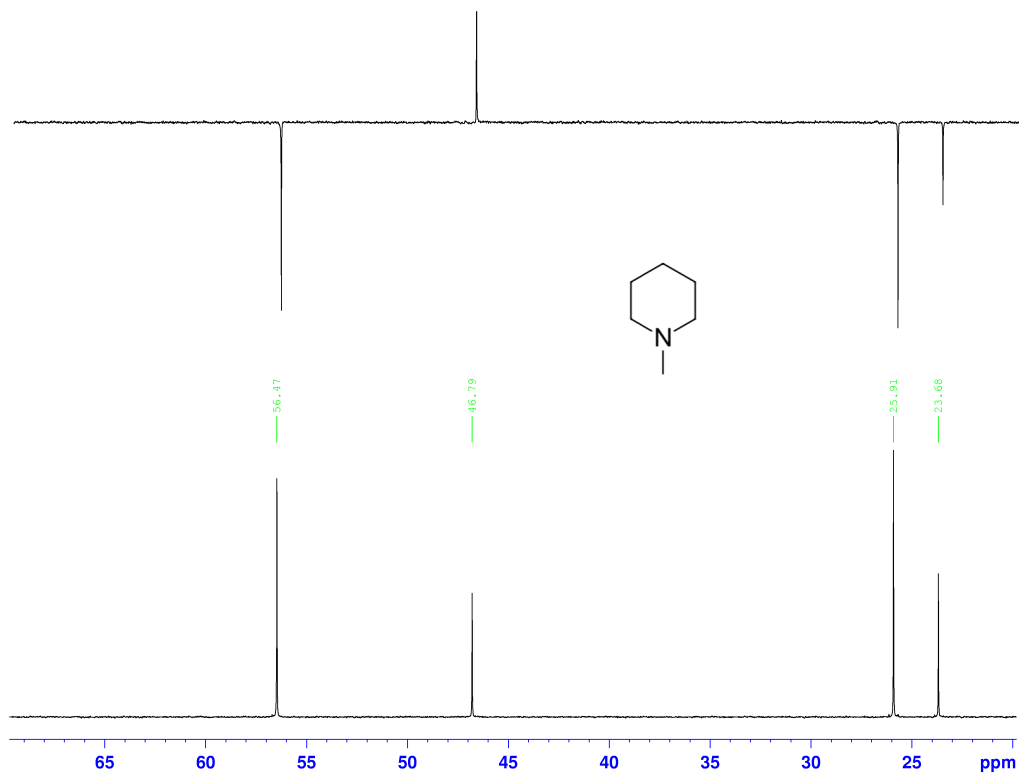


Figure 11. ¹³C and Dept 135 NMR spectra (CDCl₃) of N-methylpiperidine **8**.

The ¹³C and Dept 135 NMR spectra of N-methylpiperidine **8** exhibited four unique carbon absorption that represents the structure. The Dept 135 NMR spectrum clearly identify which peaks in the ¹³C NMR spectrum are the CH₃ and CH₂ groups. The only CH₃ group peak is at 46.79 δ which correspond to the (a). The remaining three carbon absorption can be attributed to CH₂ groups. The absorption at 56.47 δ can be attributed to the CH₂ groups that are attached to the nitrogen atom at the (b) carbons

positions. The 25.91 δ and 23.68 δ absorptions can be attributed to the remaining CH_2 groups of (c) and (d), respectively.

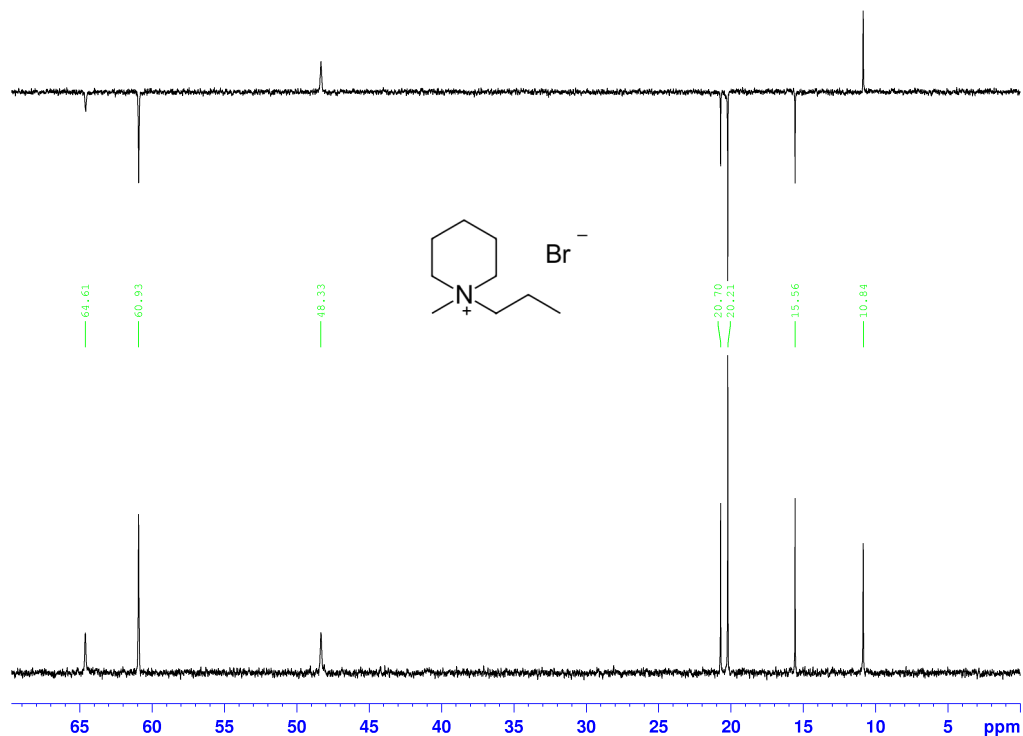


Figure 12. ^{13}C and Dept 135 NMR spectra (CDCl_3) of PIP_{13}Br **1c**.

The ^{13}C and Dept 135 NMR spectra of PIP_{13}Br **1c** exhibited seven unique carbon absorption that represents the structure. The Dept 135 NMR spectrum clearly identify which peaks in the ^{13}C NMR spectrum are the CH_3 and CH_2 groups. The only two CH_3 group peaks are at 48.32 δ and 10.85 δ which correspond to the (d) and (a), respectively. The remaining five carbon absorption can be attributed to CH_2 groups. The absorptions at 64.61 δ and 60.93 δ can be attributed to the CH_2 groups that are attached to the nitrogen atom at the (e) and (c) carbons positions, respectively. The 20.70 δ , 20.21 δ and 15.56 δ absorptions can be attributed to the remaining CH_2 groups of (f), (g) and (b), respectively.

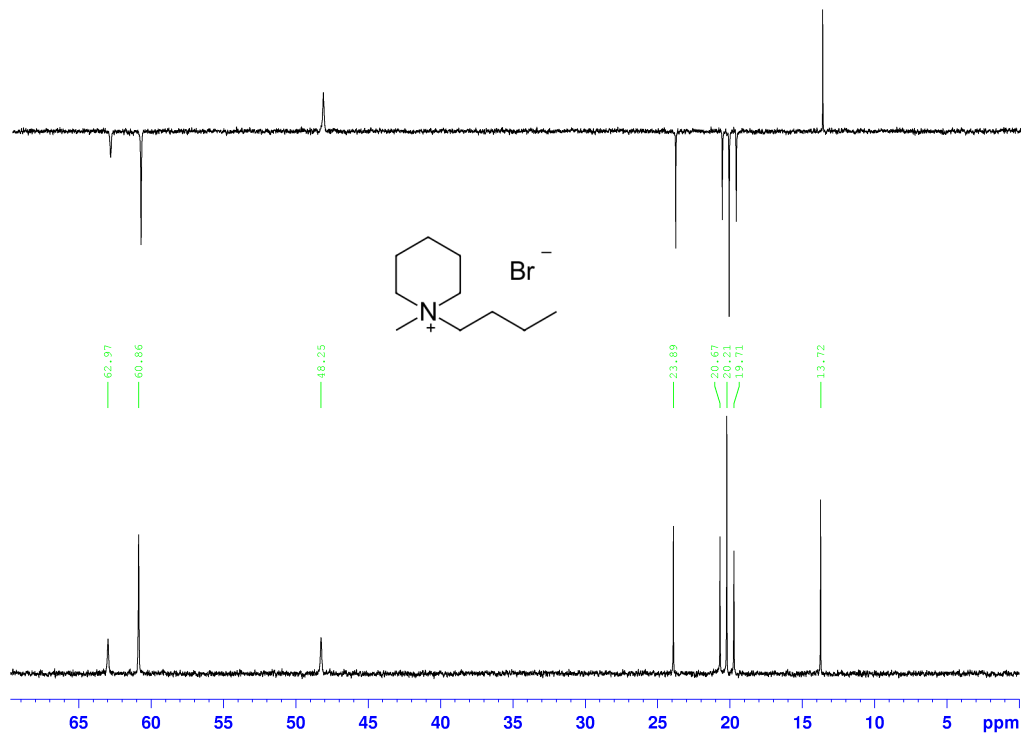


Figure 13. ^{13}C and Dept 135 NMR spectra (CDCl_3) of PIP_{14}Br **1d**.

The ^{13}C and Dept 135 NMR spectra of PIP_{13}Br **1c** exhibited eight unique carbon absorption that represents the structure. The Dept 135 NMR spectrum clearly identify which peaks in the ^{13}C NMR spectrum are the CH_3 and CH_2 groups. The only two CH_3 group peaks are at 48.25 δ and 13.73 δ which correspond to the (e) and (a), respectively. The remaining six carbon absorption can be attributed to CH_2 groups. The absorptions at 62.96 δ and 60.85 δ can be attributed to the CH_2 groups that are attached to the nitrogen atom at the (d) and (f) carbons positions, respectively. The 23.89 δ , 20.67 δ , 20.20 δ and 19.71 δ absorptions can be attributed to the remaining CH_2 groups of (g), (h), (c) and (b), respectively.

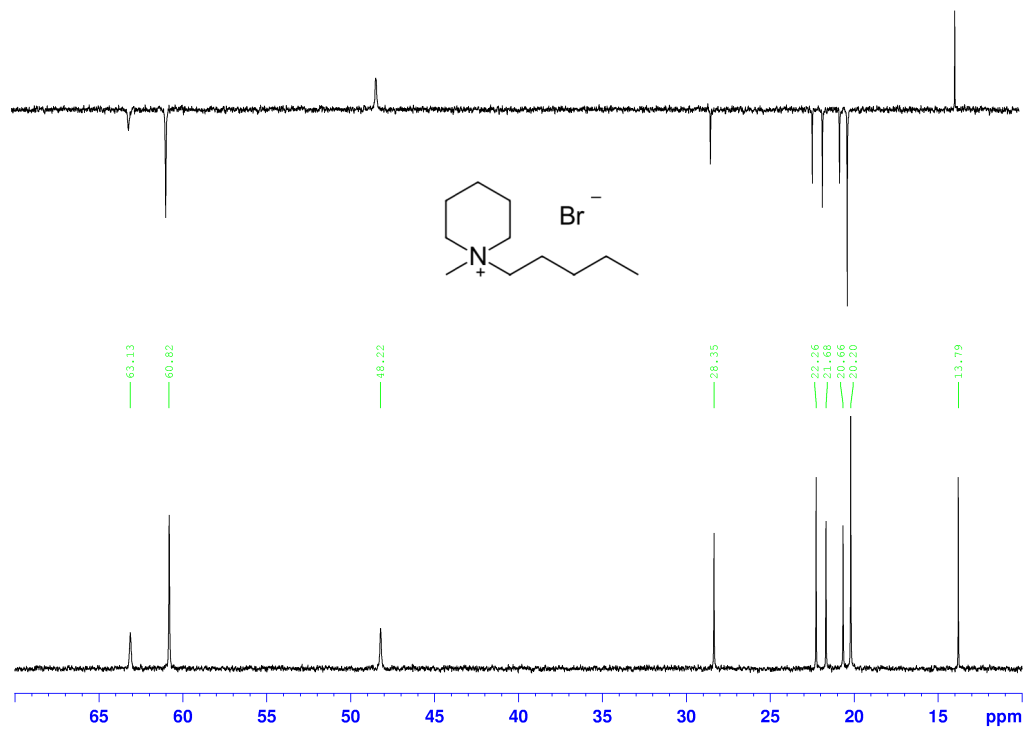


Figure 14. ^{13}C and Dept 135 NMR spectra (CDCl_3) of PIP_{15}Br **1e**.

The ^{13}C and Dept 135 NMR spectra of PIP_{13}Br **1c** exhibited nine unique carbon absorption that represents the structure. The Dept 135 NMR spectrum clearly identify which peaks in the ^{13}C NMR spectrum are the CH_3 and CH_2 groups. The only two CH_3 group peaks are at 48.32 δ and 13.81 δ which correspond to the (f) and (a), respectively. The remaining seven carbon absorption can be attributed to CH_2 groups. The absorptions at 63.05 δ and 60.83 δ can be attributed to the CH_2 groups that are attached to the nitrogen atom at the (e) and (g) carbons positions, respectively. The 28.37 δ , 22.30 δ , 21.70 δ , 20.68 δ and 20.22 δ absorptions can be attributed to the remaining CH_2 groups of (h), (i), (d), (c) and (b), respectively.

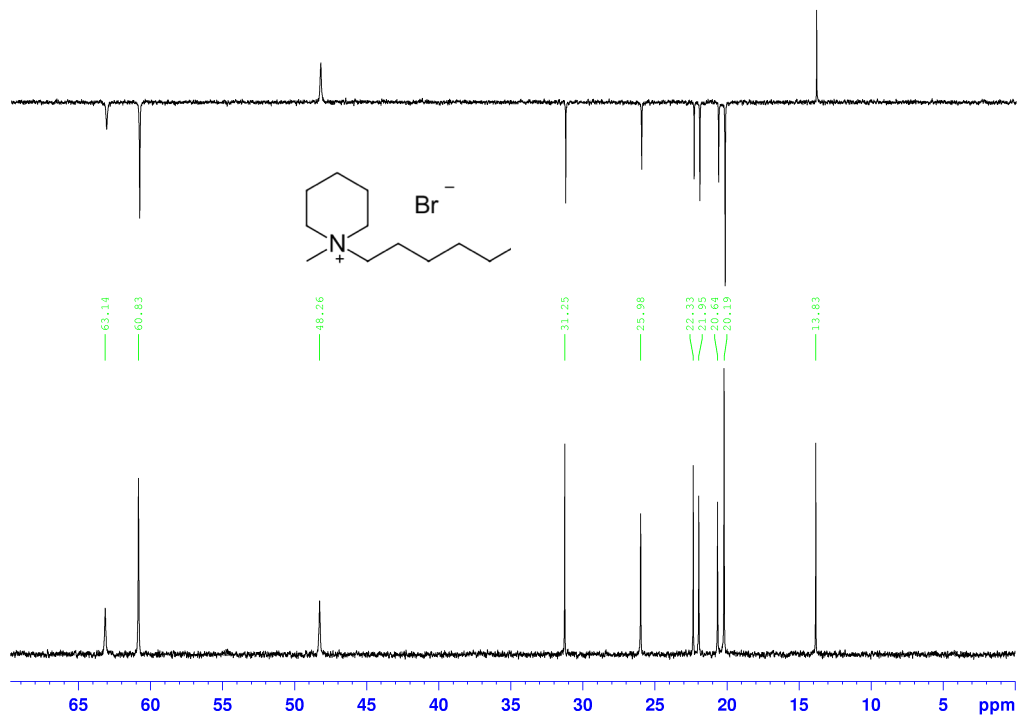


Figure 15. ^{13}C and Dept 135 NMR spectra (CDCl_3) of PIP_{16}Br **1f**.

The ^{13}C and Dept 135 NMR spectra of PIP_{13}Br **1c** exhibited ten unique carbon absorption that represents the structure. The Dept 135 NMR spectrum clearly identify which peaks in the ^{13}C NMR spectrum are the CH_3 and CH_2 groups. The only two CH_3 group peaks are at 48.26 δ and 13.84 δ which correspond to the (g) and (a), respectively. The remaining eight carbon absorption can be attributed to CH_2 groups. The absorptions at 63.12 δ and 60.82 δ can be attributed to the CH_2 groups that are attached to the nitrogen atom at the (f) and (h) carbons positions, respectively. The 31.26 δ , 25.98 δ , 22.34 δ , 21.95 δ , 20.64 δ and 20.19 δ absorptions can be attributed to the remaining CH_2 groups of (i), (j), (e), (d), (c) and (b), respectively.

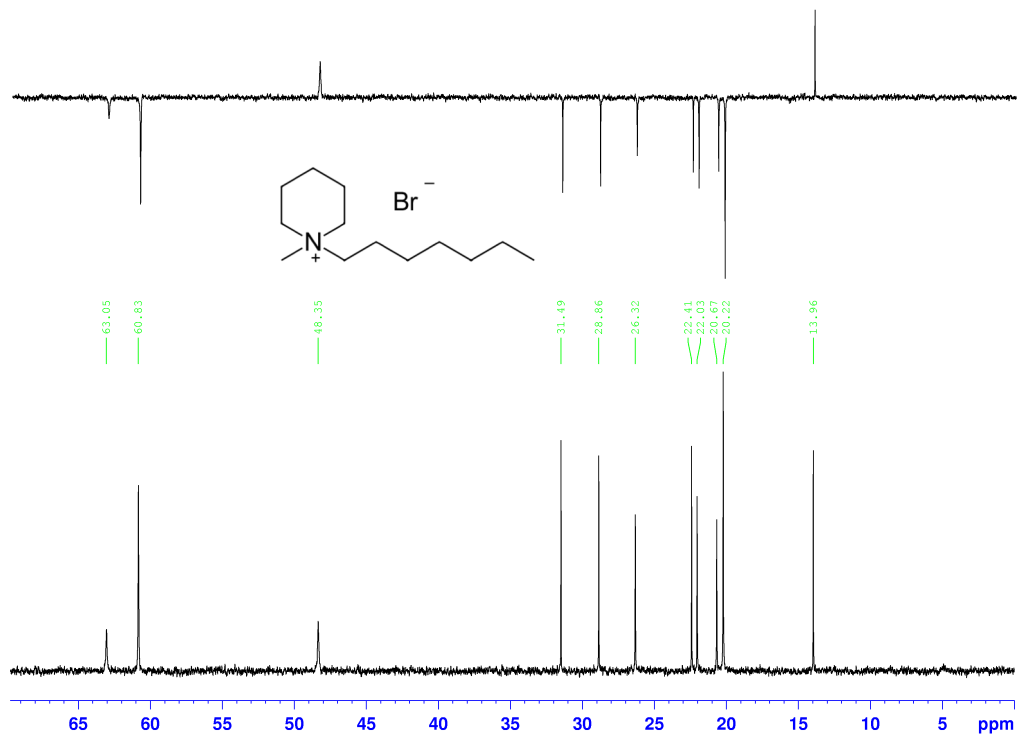


Figure 16. ^{13}C and Dept 135 NMR spectra (CDCl_3) of PIP₁₇Br **1g**.

The ^{13}C and Dept 135 NMR spectra of PIP₁₃Br **1c** exhibited eleven unique carbon absorption that represents the structure. The Dept 135 NMR spectrum clearly identify which peaks in the ^{13}C NMR spectrum are the CH_3 and CH_2 groups. The only two CH_3 group peaks are at 48.35 δ and 13.97 δ which correspond to the (h) and (a), respectively. The remaining nine carbon absorption can be attributed to CH_2 groups. The absorptions at 63.05 δ and 60.83 δ can be attributed to the CH_2 groups that are attached to the nitrogen atom at the (g) and (i) carbons positions, respectively. The 31.49 δ , 28.87 δ , 26.32 δ , 22.42 δ , 22.03 δ , 20.66 δ and 20.21 δ absorptions can be attributed to the remaining CH_2 groups of (j), (k), (f), (e), (d), (c) and (b), respectively.

IR Spectroscopy

The IR spectra were performed using NaCl salt plates for PIP_nBr **1c-g** samples.

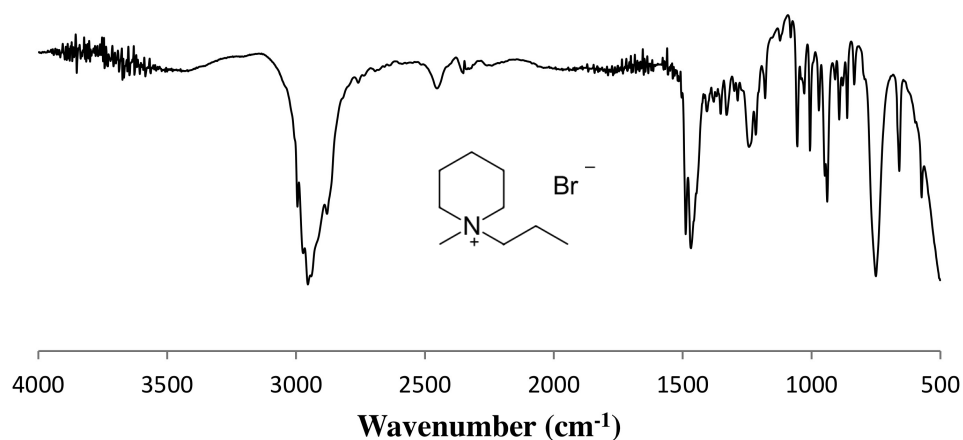


Figure 17. IR (NaCl plate) spectrum of PIP₁₃Br **1c**.

The IR spectrum of PIP₁₃Br **1c** has characteristic absorption at 2954 and 1468 cm⁻¹. The absorption peak at 2957 cm⁻¹ is the C-H bond stretching. The 1468 cm⁻¹ absorption peak is the C-H bond bending.

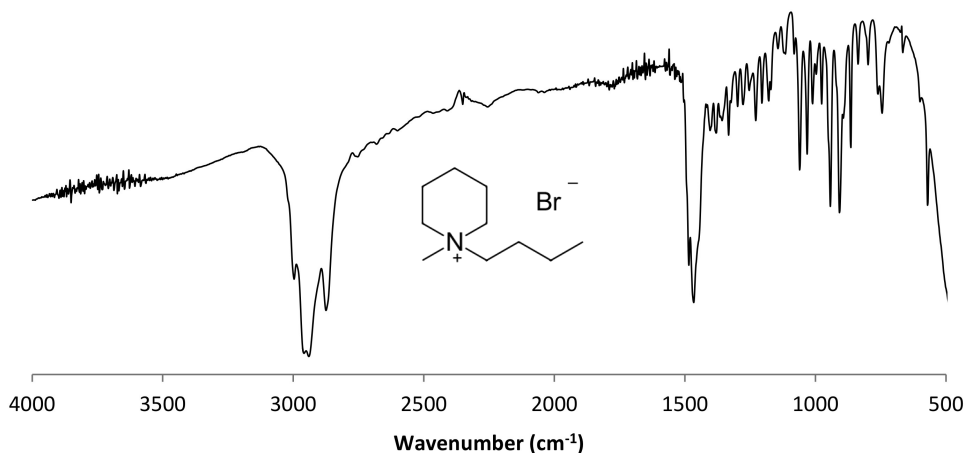


Figure 18. IR (NaCl plate) spectrum of PIP₁₄Br **1d**.

The IR spectrum of PIP₁₄Br **1d** has characteristic absorption at 2954 and 1468 cm⁻¹. The absorption peak at 2957 cm⁻¹ is the C-H bond stretching. The 1468 cm⁻¹ absorption peak is the C-H bond bending.

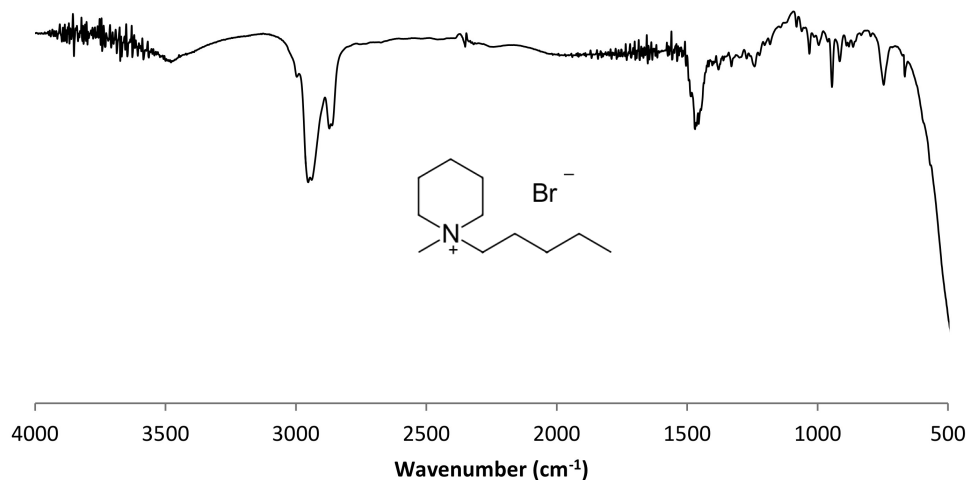


Figure 19. IR (NaCl plate) spectrum of PIP₁₅Br **1e**.

The IR spectrum of PIP₁₅Br **1e** has characteristic absorption at 2954 and 1468 cm⁻¹. The absorption peak at 2957 cm⁻¹ is the C-H bond stretching. The 1468 cm⁻¹ absorption peak is the C-H bond bending.

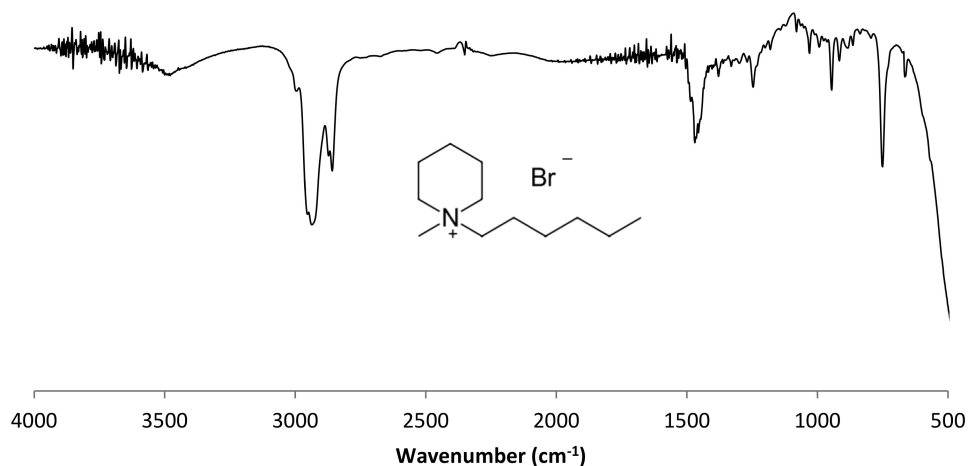


Figure 20. IR (NaCl plate) spectrum of PIP₁₆Br **1f**.

The IR spectrum of PIP₁₆Br **1f** has characteristic absorption at 2954 and 1468 cm⁻¹. The absorption peak at 2957 cm⁻¹ is the C-H bond stretching. The 1468 cm⁻¹ absorption peak is the C-H bond bending.

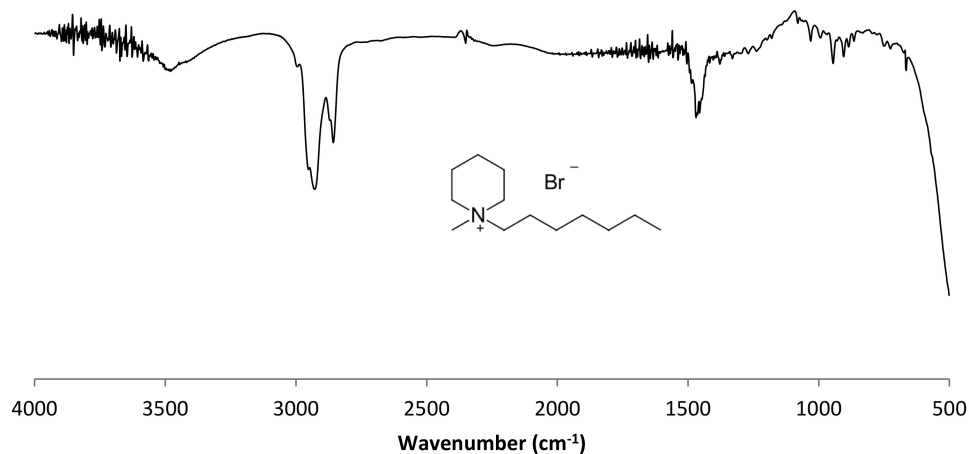


Figure 21. IR (NaCl plate) spectrum of PIP₁₇Br **1g**.

The IR spectrum of PIP₁₇Br **1g** has characteristic absorption at 2954 and 1468 cm⁻¹. The absorption peak at 2957 cm⁻¹ is the C-H bond stretching. The 1468 cm⁻¹ absorption peak is the C-H bond bending.

Thermal Gravimetric Analysis

The thermal stability of the exchange products **24** and **25** were determined by thermal gravimetric analysis (TGA), using a 20°/min ramp. Both TGA were performed using nitrogen and oxygen atmosphere.

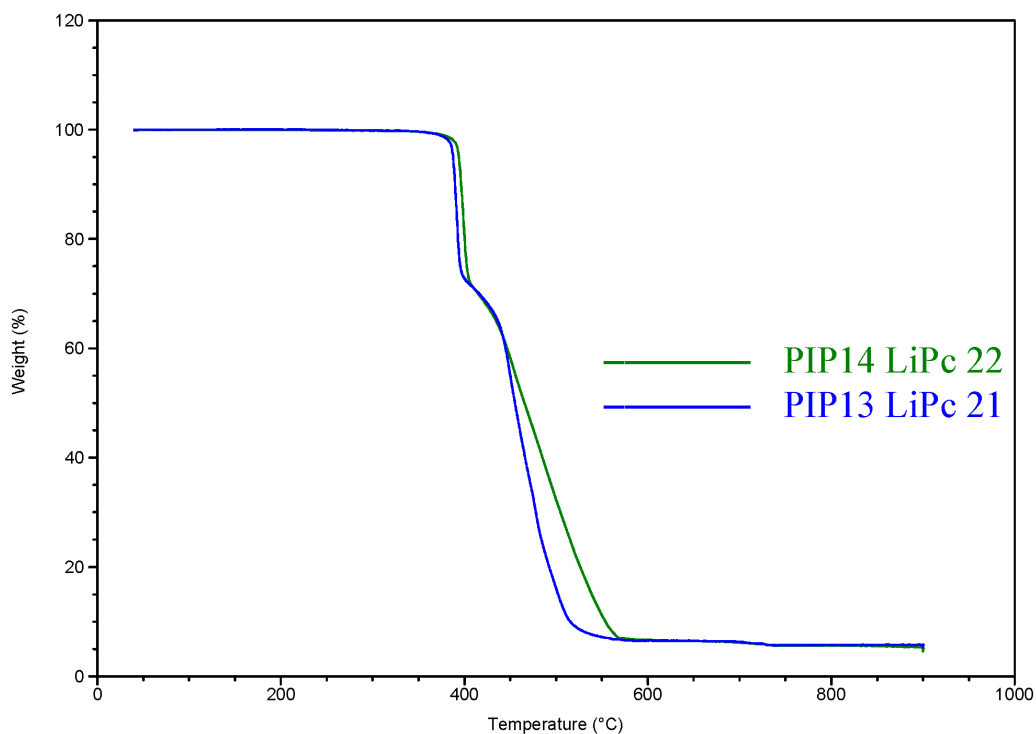


Figure 22. Weight % vs. temperature TGA overlay of **21** and **22**.

The thermal stability of the exchange products **21** and **22** were very similar. The weight loss for both exchange products at 450° was about 74% and 72% of **21** and **22** original mass, respectively. The TGA appears to be governed by the PIP_{1(3&4)} cation.

Differential Scanning Calorimetry

The phase transitions of the PIP_{1n}Br **1c-g** exchange products **21** and **22** were examined by differential scanning calorimetry (DSC), using a 10°/min ramp for two heating scan and 20°/min for the cooling scan. All the DSC were performed using nitrogen atmosphere.

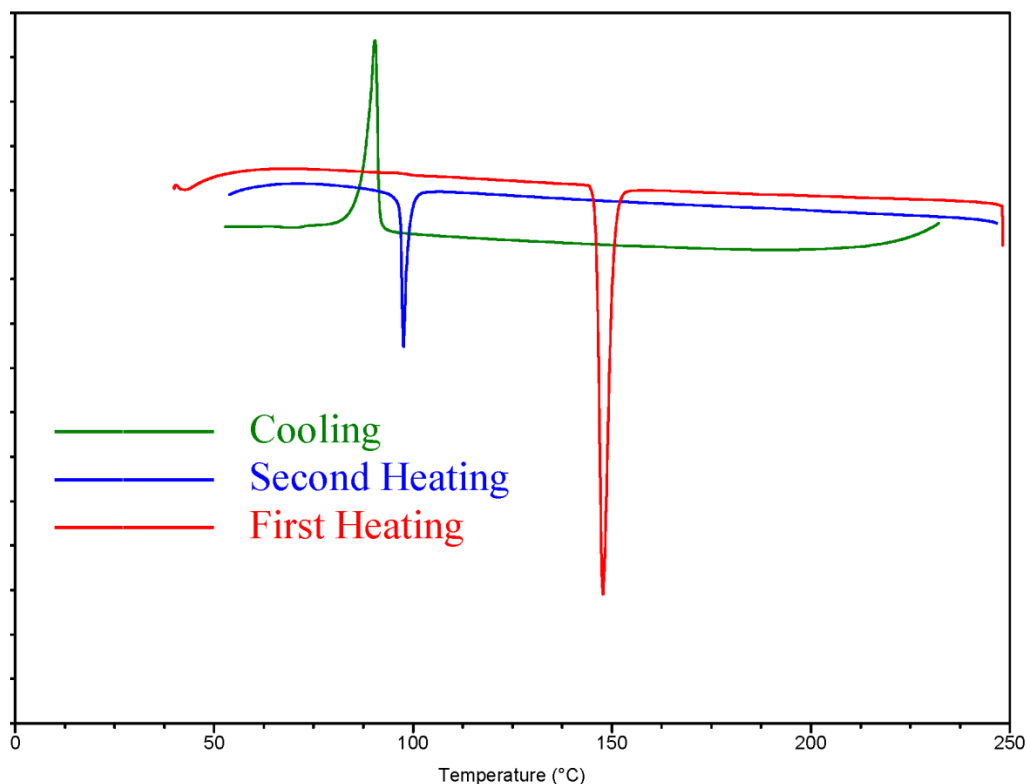


Figure 23. DSC trace of PIP₁₃Br **1c**.

The DSC traces of the product PIP₁₃Br **1c** appeared to show transitions in the product initial heating scan. During the initial heating the product appeared to undergo two endothermic transitions at 148° and 250°. The first endothermic peak would suggest the product was undergoing solid-solid transition, while the second peak can be attributed to the sample melting. On the cooling scan an exothermic peak was seen, which would suggest crystallization at 90°. On the second heating scan an endothermic peak was seen, which would suggest melting at 96°.

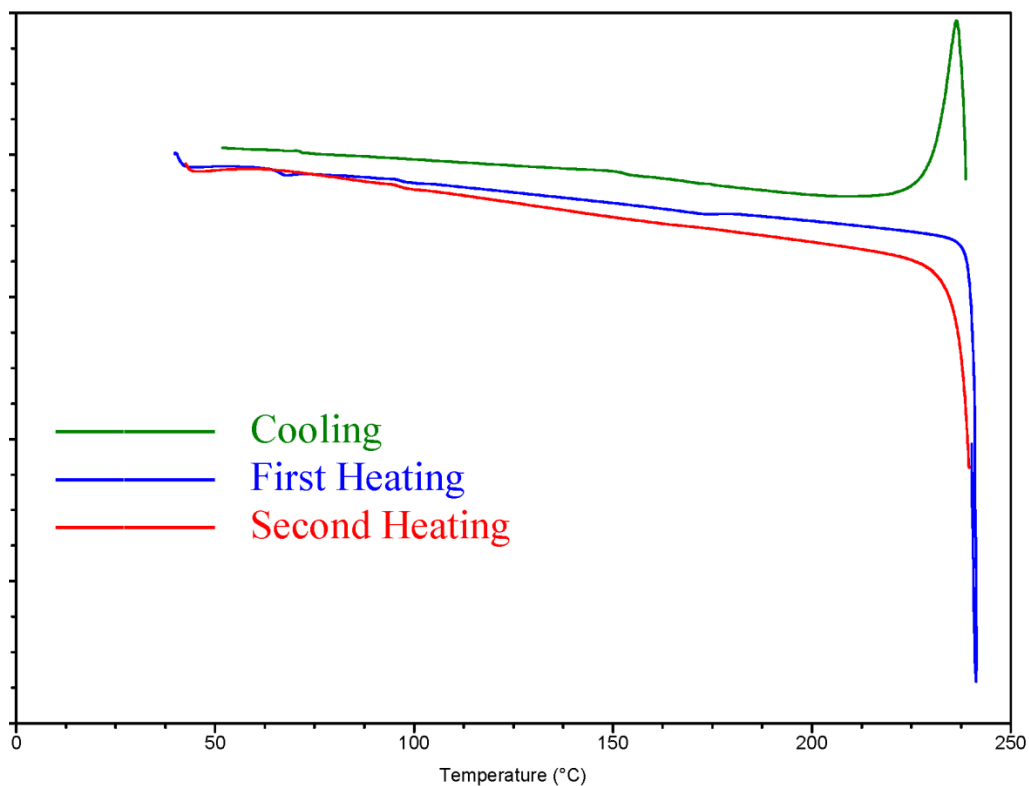


Figure 24. DSC trace of PIP₁₄Br **1d**.

The DSC traces of the product PIP₁₄Br **1d** appeared to show transitions in the product initial heating scan. During the initial heating the product appeared to undergo endothermic transitions at 240°, which can be attributed to the sample melting. On the cooling scan an exothermic peak was seen, which would suggest crystallization at 230°. On the second heating scan an endothermic peak was seen, which can be attributed to the sample melting at 240°.

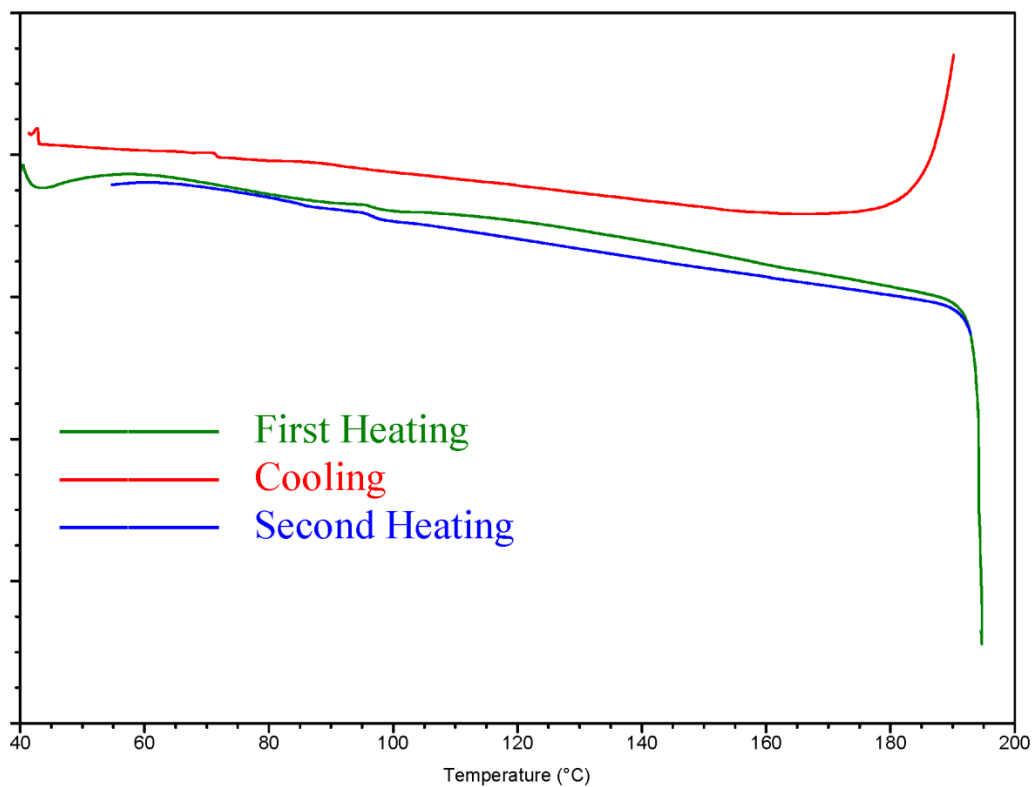


Figure 25. DSC trace of PIP₁₅Br **1e**.

The DSC traces of the product PIP₁₅Br **1e** appeared to show transitions in the product initial heating scan. During the initial heating the product appeared to undergo endothermic transitions at 195°, which can be attributed to the sample melting. On the cooling scan an exothermic peak was seen, which would suggest crystallization at 191°. On the second heating scan an endothermic peak was seen, which can be attributed to the sample melting at 195°.

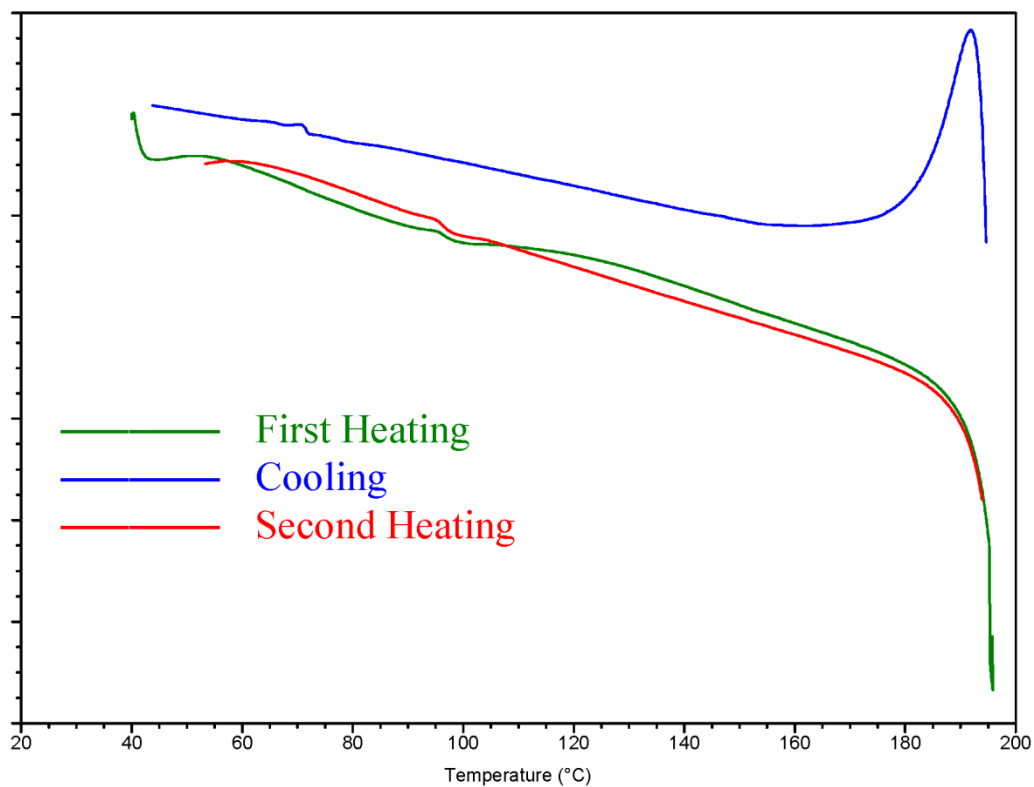


Figure 26. DSC trace of PIP₁₆Br **1f**.

The DSC traces of the product PIP₁₆Br **1f** appeared to show transitions in the product initial heating scan. During the initial heating the product appeared to undergo endothermic transitions at 196°, which can be attributed to the sample melting. On the cooling scan an exothermic peak was seen, which would suggest crystallization at 190°. On the second heating scan an endothermic peak was seen, which can be attributed to the sample melting at 196°.

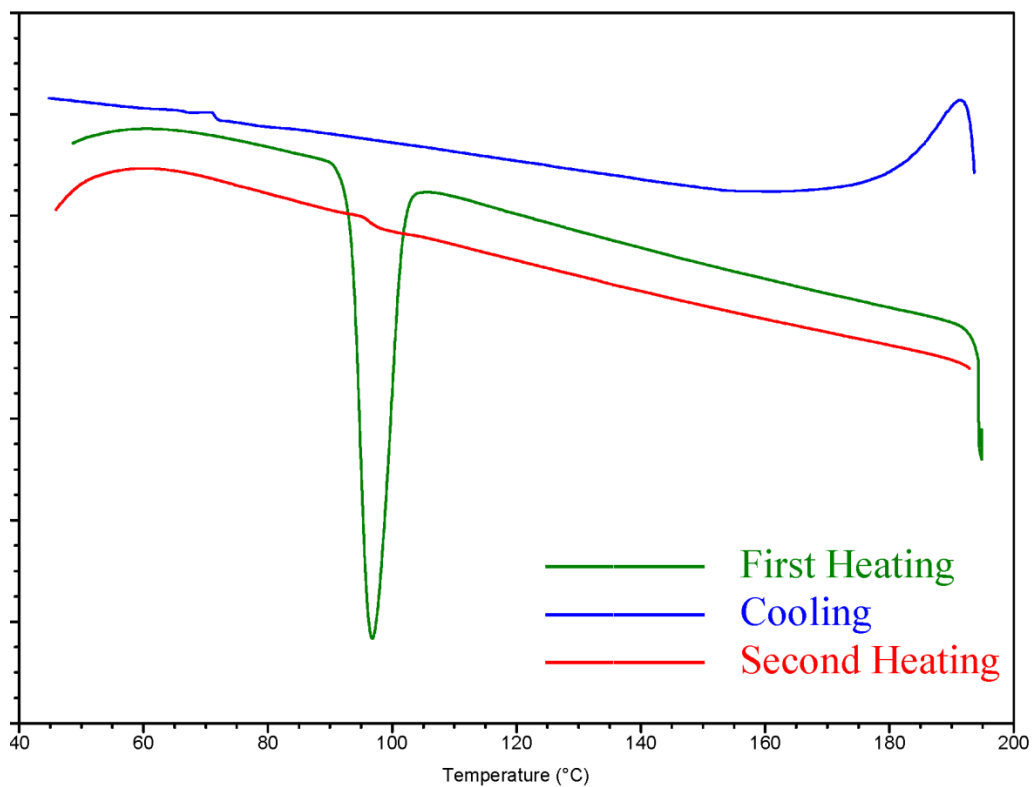


Figure 27. DSC trace of PIP₁₇Br **1g**.

The DSC traces of the product PIP₁₇Br **1g** appeared to show transitions in the product initial heating scan. During the initial heating the product appeared to undergo two endothermic transitions at 95° and 195°. The first endothermic peak would suggest the product was undergoing solid-solid transition, while the second peak can be attributed to the sample melting. On the cooling scan an exothermic peak was seen, which would suggest crystallization at 188°. On the second heating scan, there appears to be no transitions peaks suggesting the product did not melt.

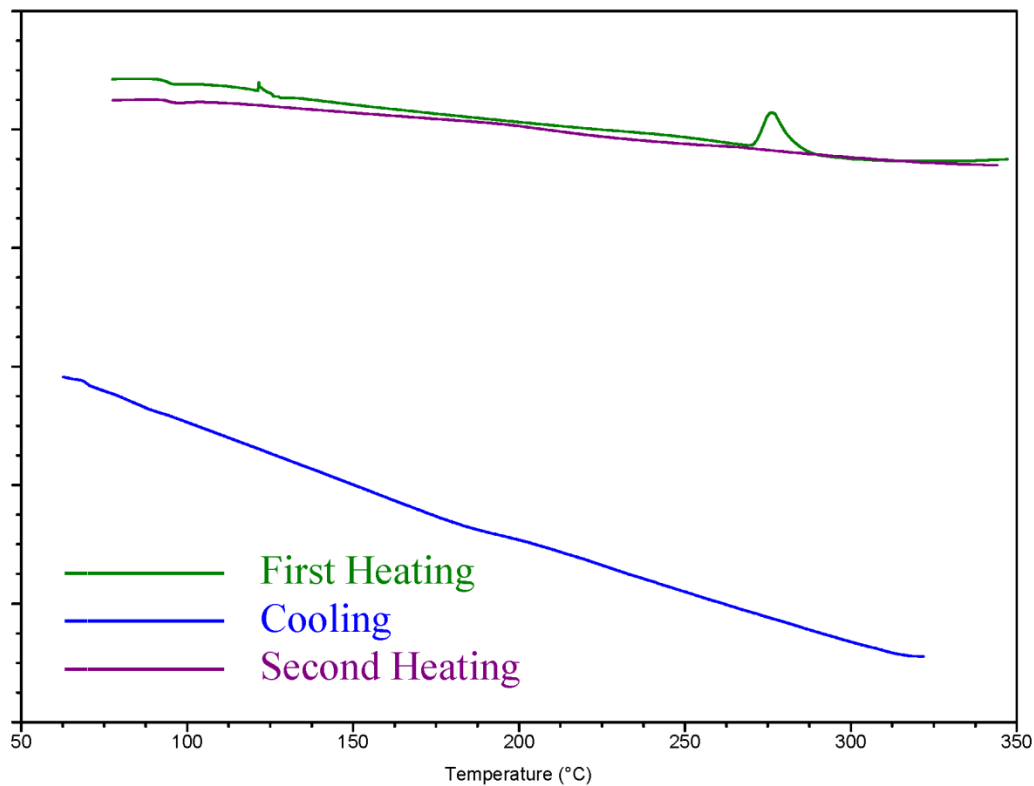


Figure 28. DSC trace of PIP₁₃ LiPc **21**.

The DSC traces of the product PIP₁₃ LiPc **21** appeared to show transitions in the product initial heating scan. During the initial heating the scan appeared to undergo two exothermic transitions at 121° and 278°. Exothermic would suggest the product was undergoing crystallizing. During the cooling and second heating scan, it appeared there were no observed transition peaks indicating that the product did not re-crystallize or melt. Which would suggest the product is morph.

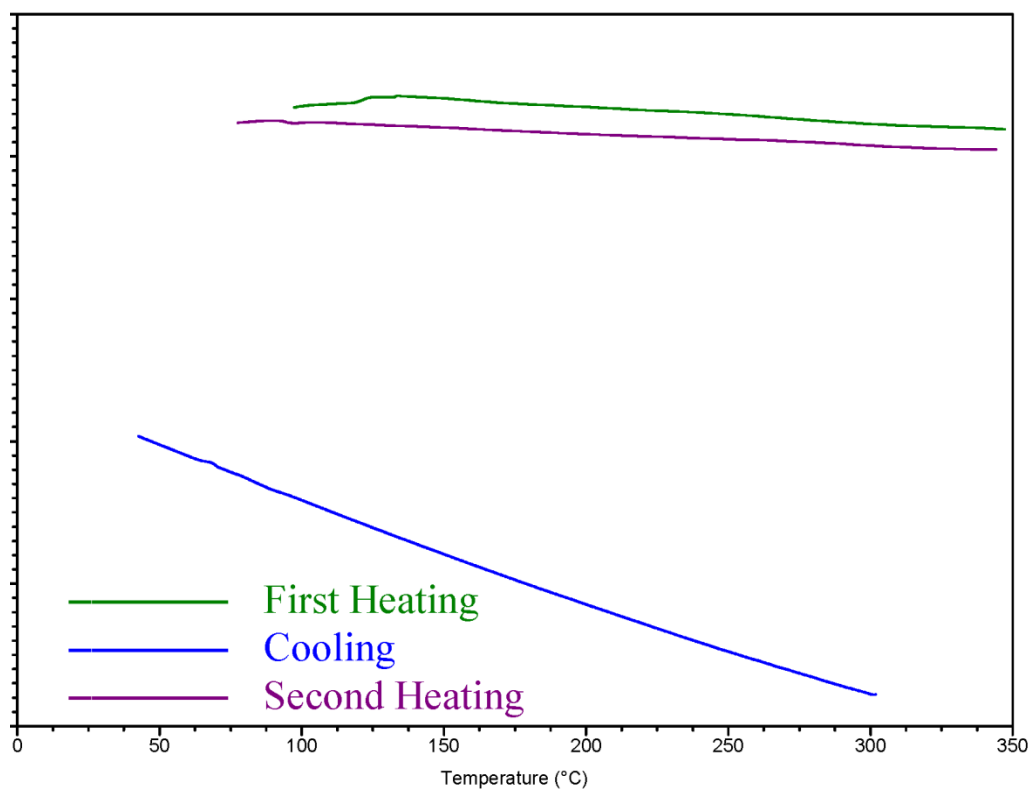


Figure 29. DSC trace of PIP₁₄ LiPc **22**.

The DSC traces of the product PIP₁₄ LiPc **22** appeared to show no transition peaks in the product initial heating, cooling or second heating scan suggesting the product is morph.

Conclusions

The N-methyl-N-alkylpiperidinium bromide **1** series was successfully synthesized by nucleophilic substitution of the alkylbromide by **8**, using the solvent free method developed. A few of the salts **1c** and **1d** were then used in the exchange reaction with **2**. The remaining salts were not completed with the exchange reaction due to funding being stopped.

The ^1H NMR spectra were obtained for the salts series and the exchange products. It was found that the spectrum clearly shows identifying peaks for the structures. However, the spectrum does not clearly identify each proton position. The salts were obtained in high yields ranging from 91.73% to 85%, while the exchange products yields were PIP₁₄ LiPc 84.65% and PIP₁₃ LiPc 78.53%.

The elemental analysis for the salts and exchange products were in the acceptable range for the calculated and found values for carbon, hydrogen and nitrogen for publishable results. The melting points of the salts were found ranging from 190.6° to 250.9°. The exchange products were found to be thermally stable to 350°.

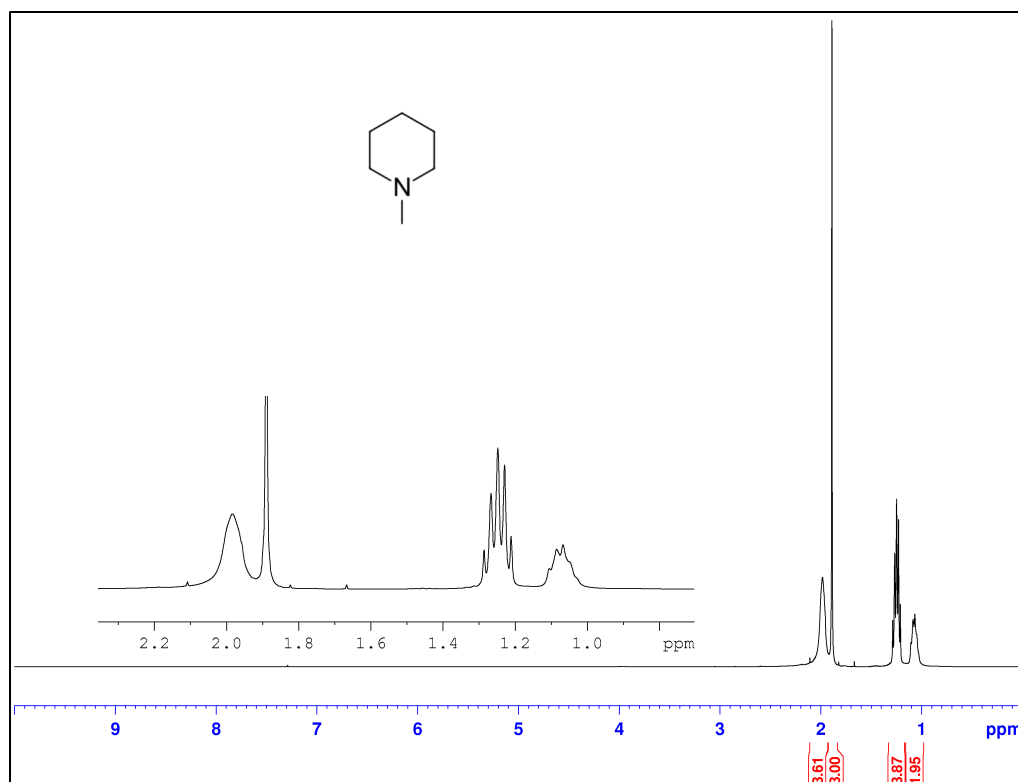


Figure 30. 300 MHz ^1H NMR spectrum (CDCl_3) of **8**.

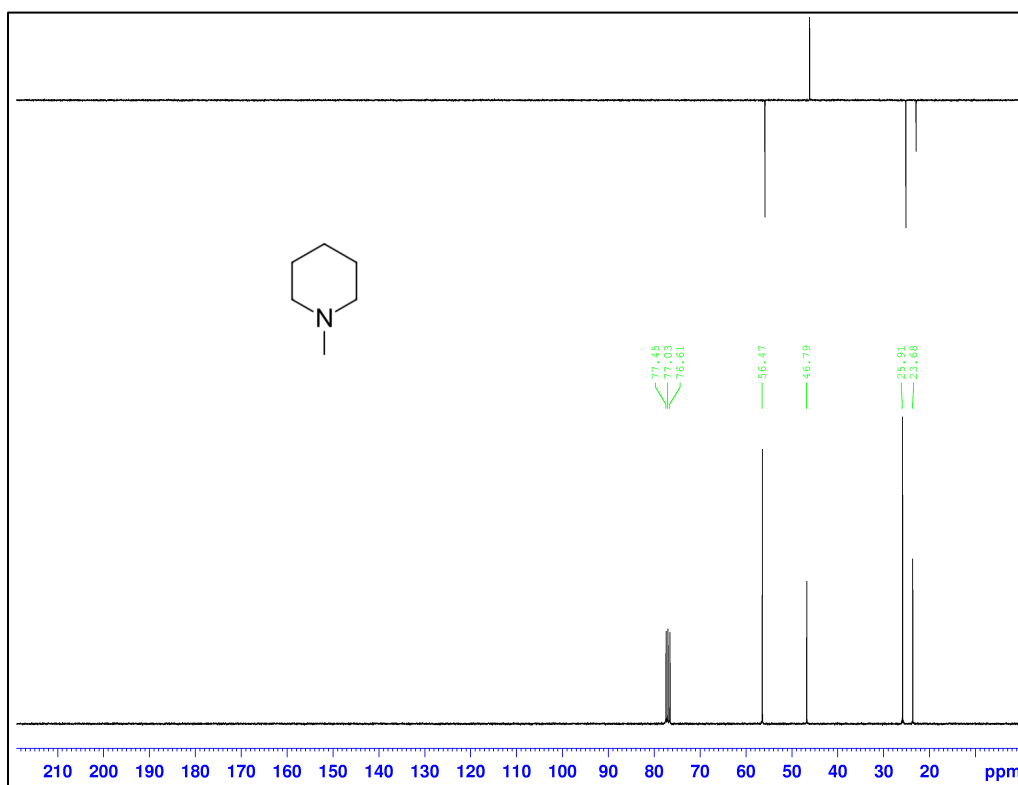


Figure 31. 75 MHz ^{13}C and Dept 135 NMR spectra (CDCl_3) of **8**.

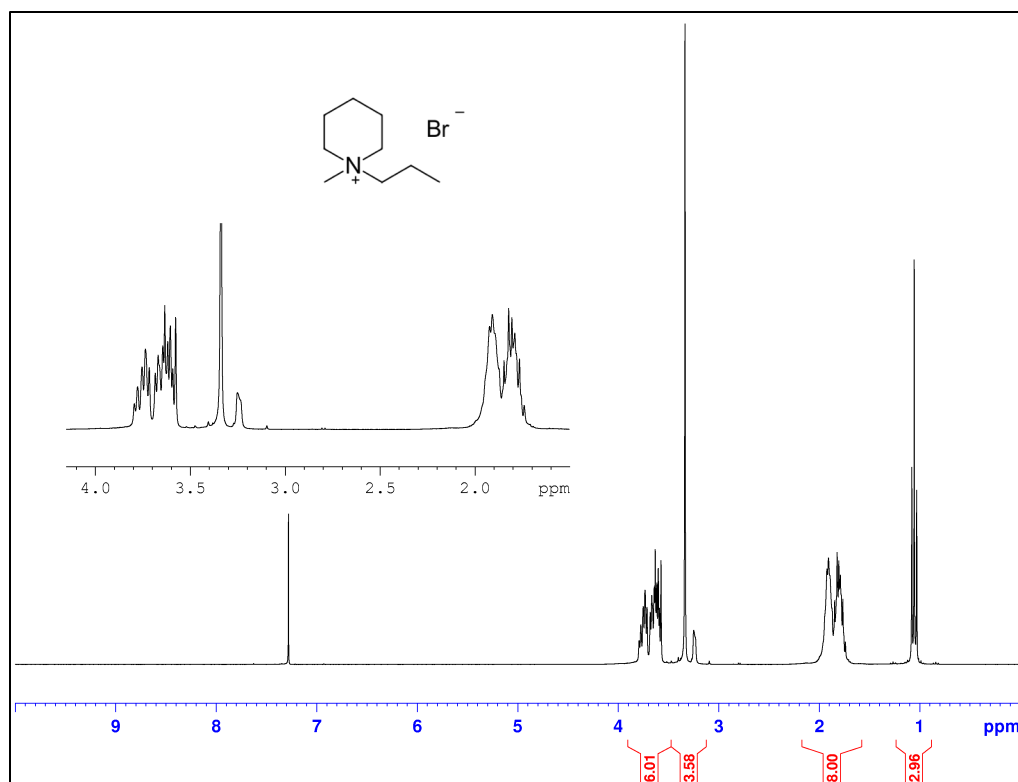


Figure 32. 300 MHz ¹H NMR spectrum (CDCl₃) of PIP₁₃Br 1c.

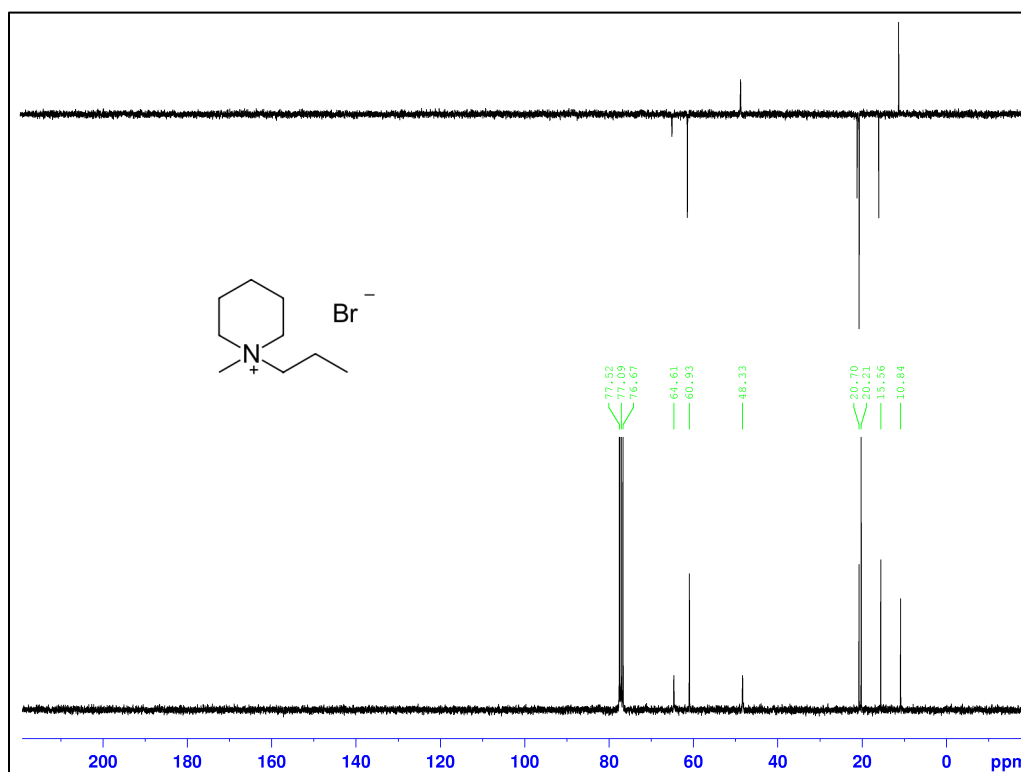


Figure 33. 75 MHz ¹³C and Dept 135 NMR spectra (CDCl₃) of PIP₁₃Br 1c.

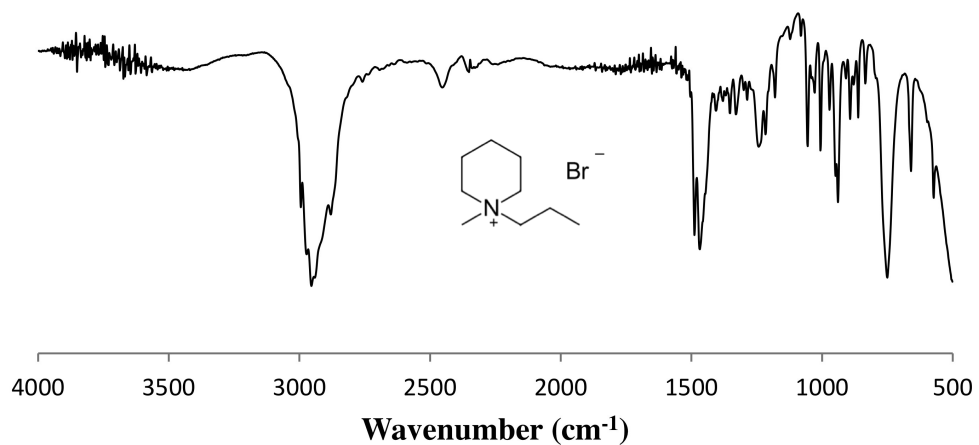


Figure 34. IR (NaCl plate) spectrum of PIP₁₃Br **1c**.

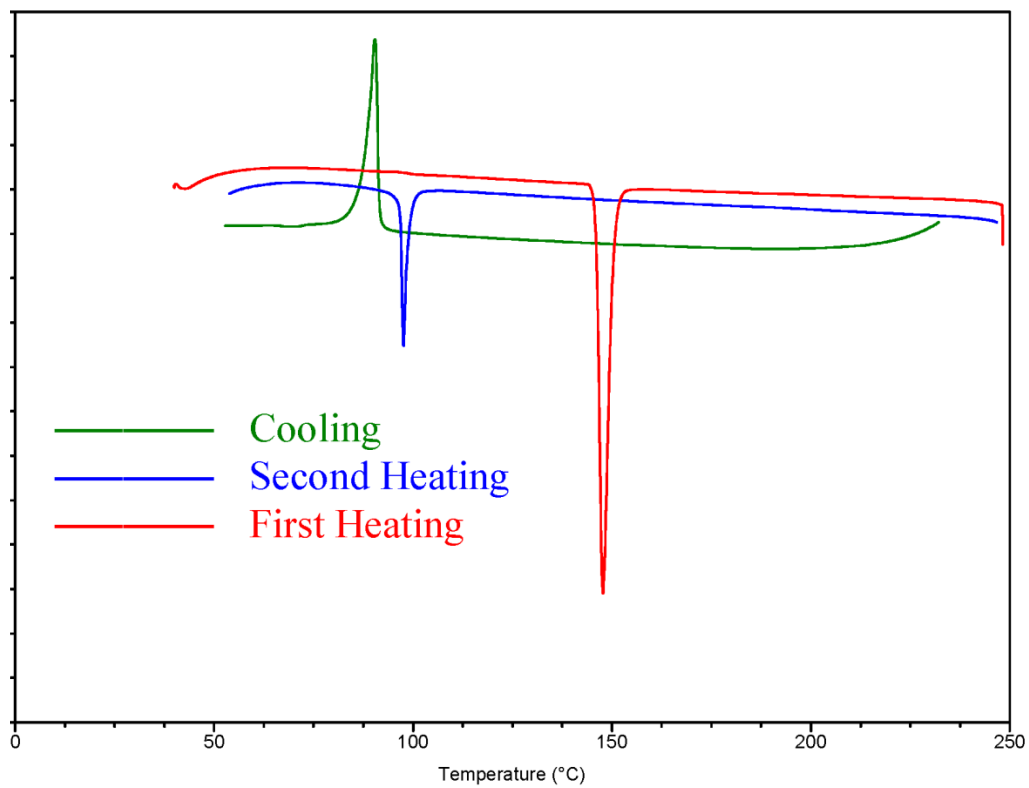


Figure 35. DSC trace of PIP₁₃Br **1c**.

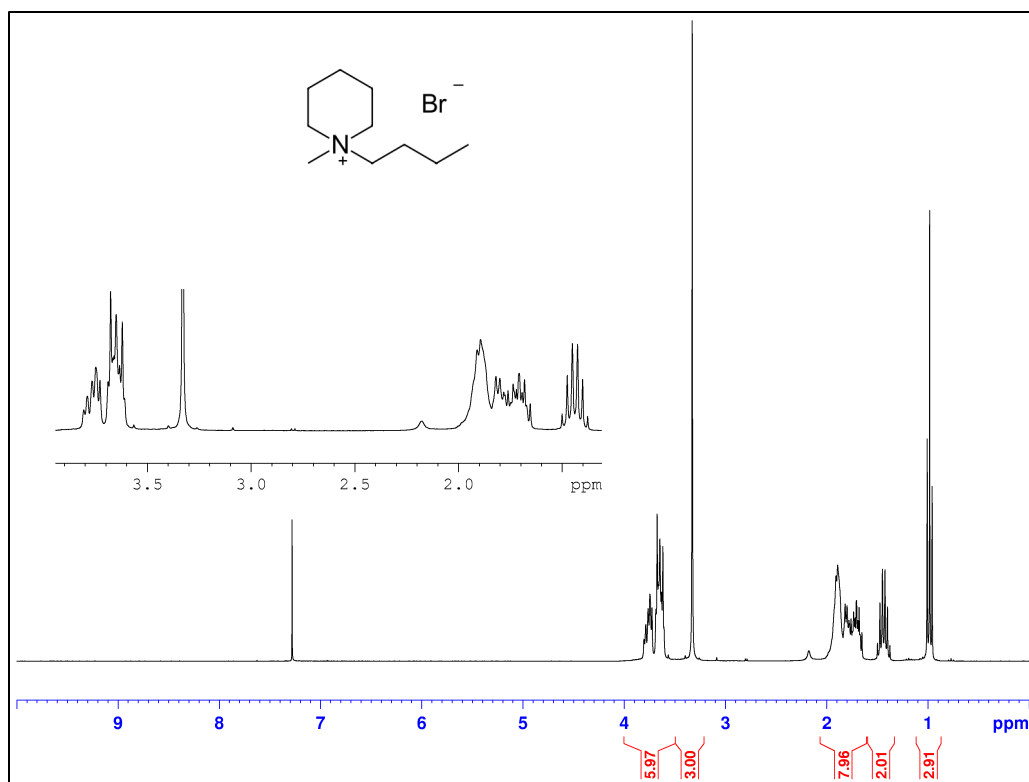


Figure 36. 300 MHz ^1H NMR spectrum (CDCl_3) of PIP₁₄Br **1d**.

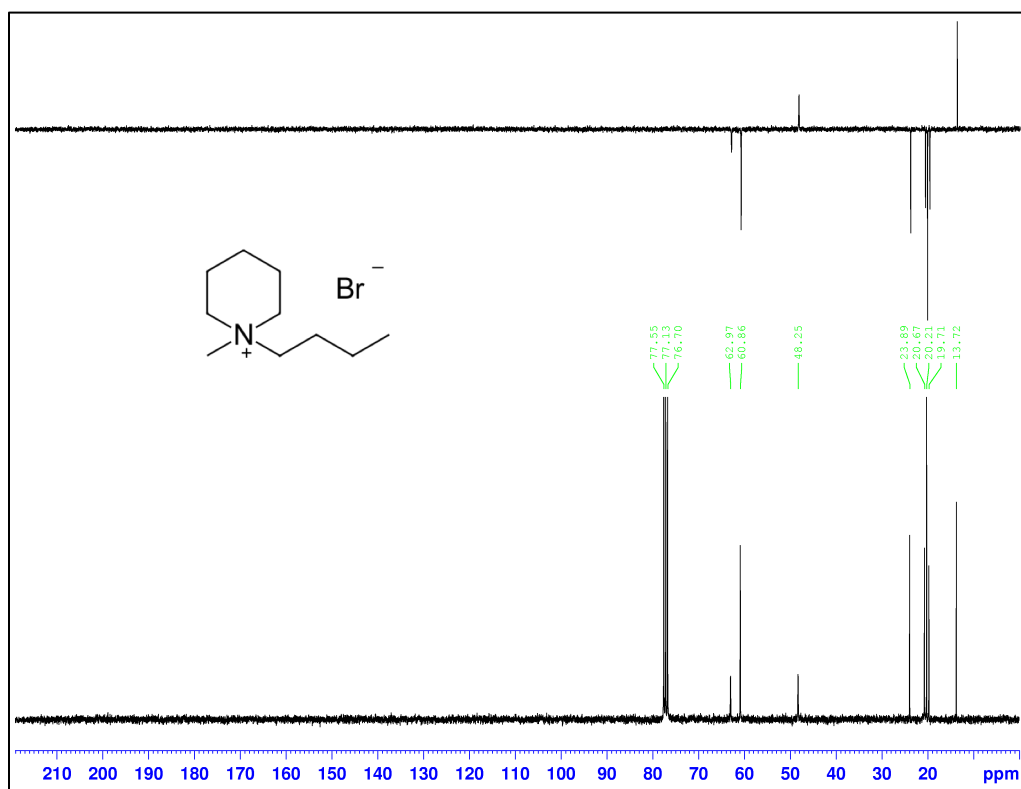


Figure 37. 75 MHz ^{13}C and Dept 135 NMR spectra (CDCl_3) of PIP₁₄Br **1d**.

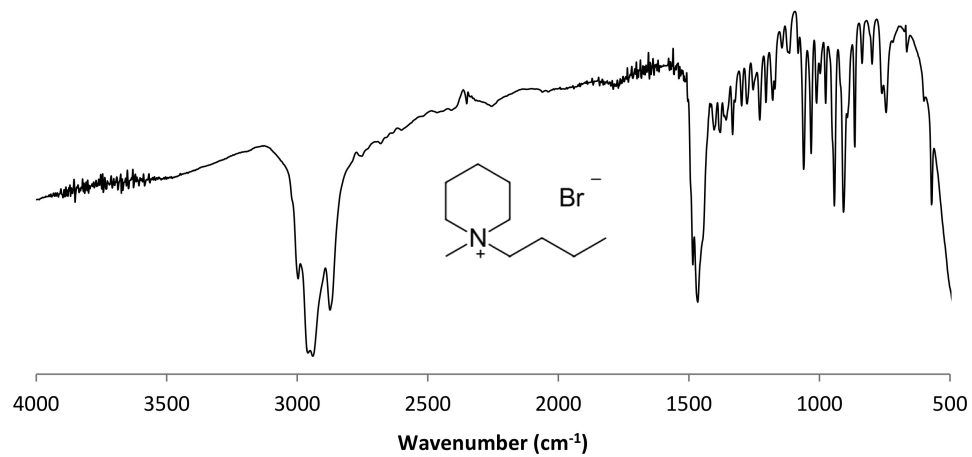


Figure 38. IR (NaCl plate) spectrum of PIP₁₄Br **1d**.

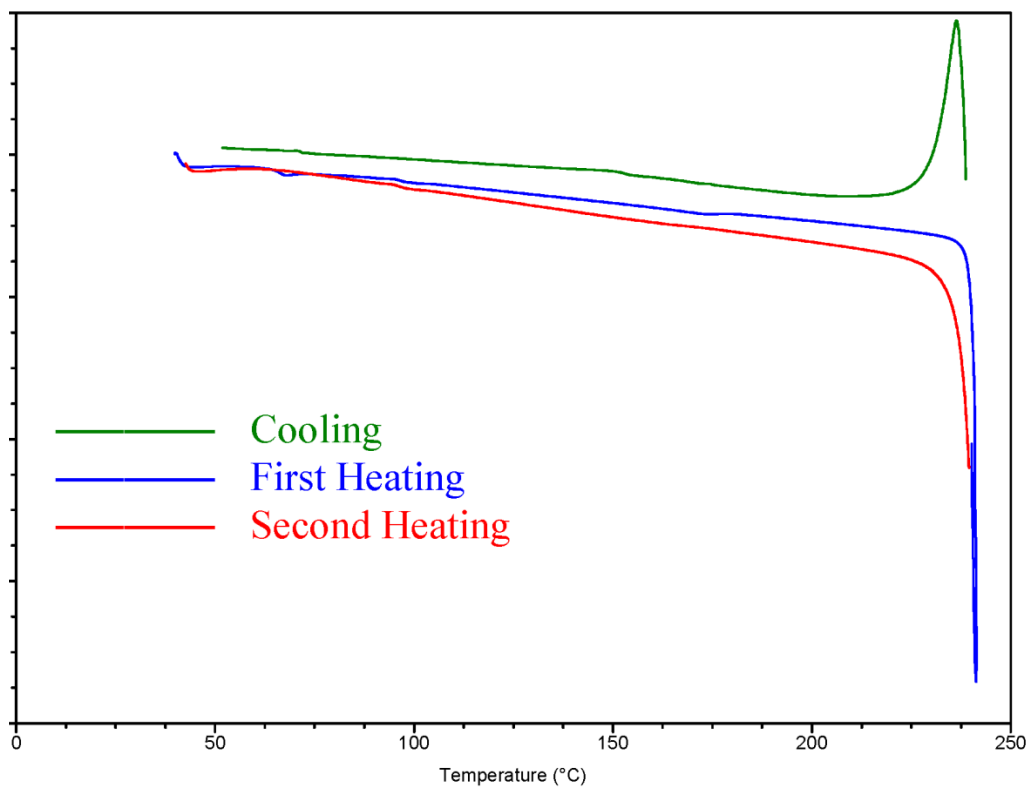


Figure 39. DSC trace of PIP₁₄Br **1d**.

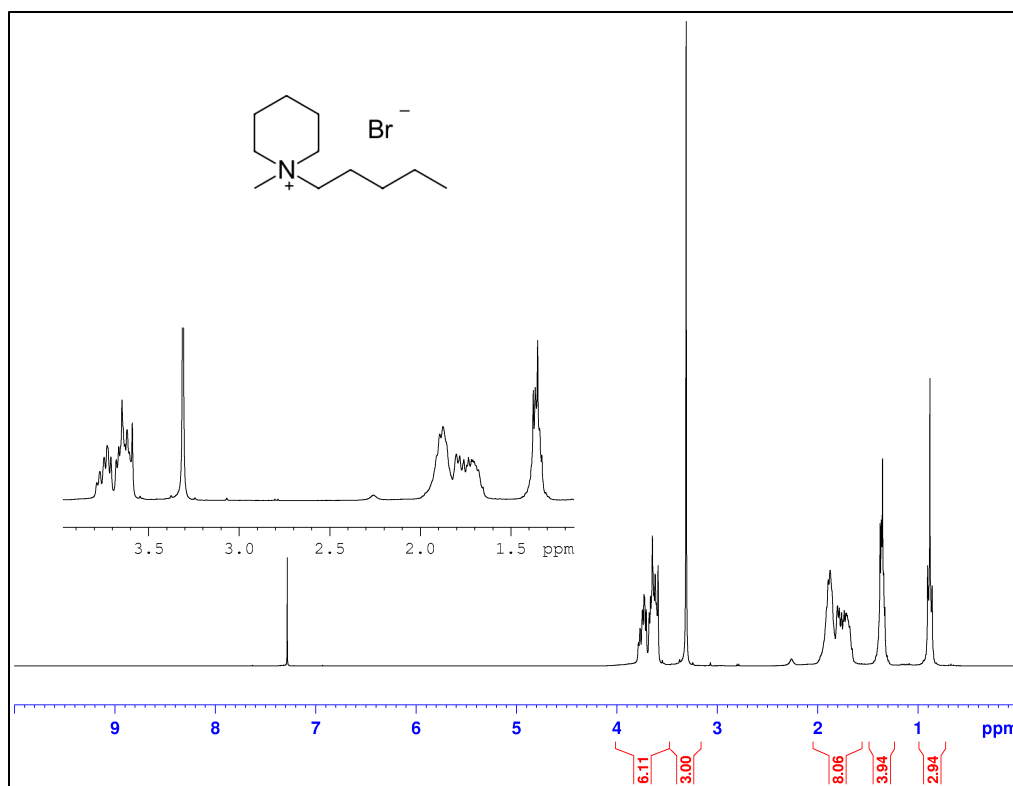


Figure 40. 300 MHz ^1H NMR spectrum (CDCl_3) of PIP_{15}Br **1e**.

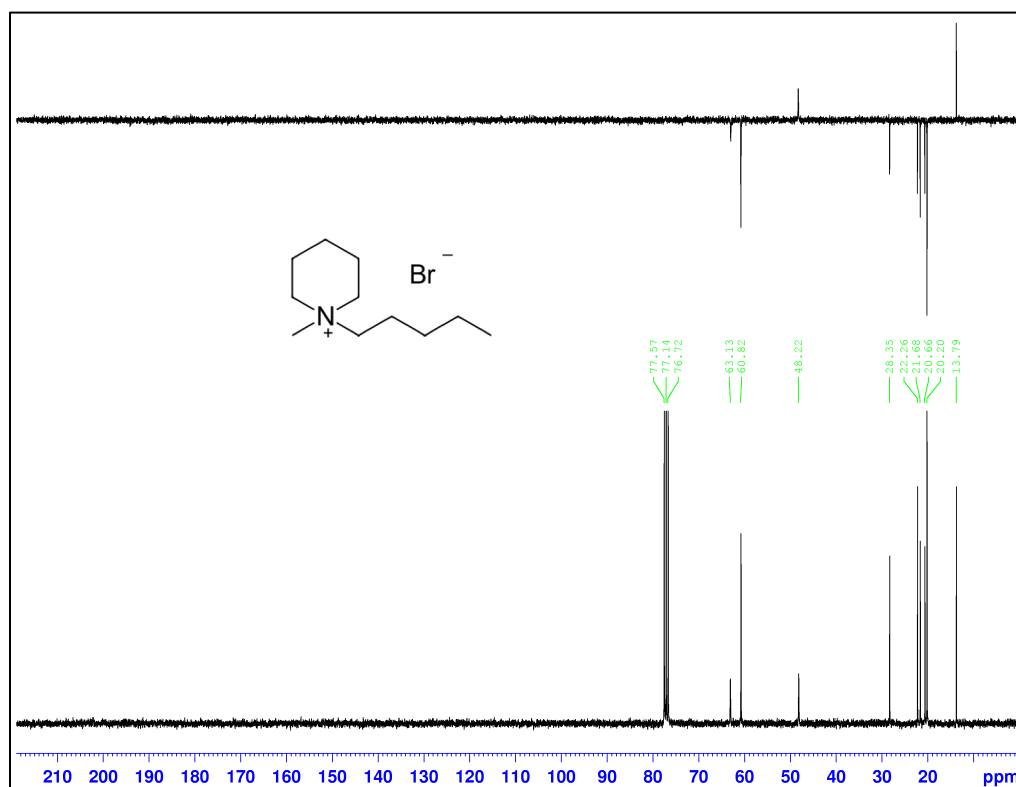


Figure 41. 75 MHz ^{13}C and Dept 135 NMR spectra (CDCl_3) of PIP_{15}Br **1e**.

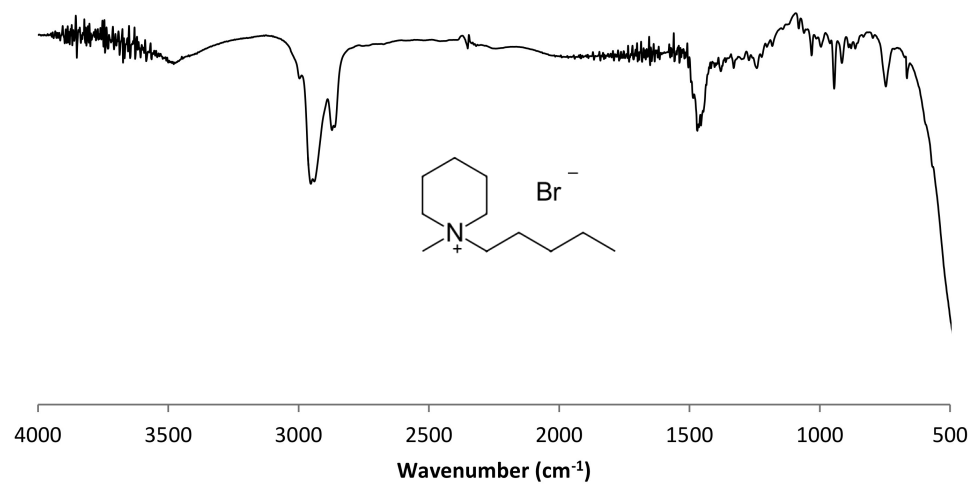


Figure 42. IR (NaCl plate) spectrum of PIP₁₅Br **1e**.

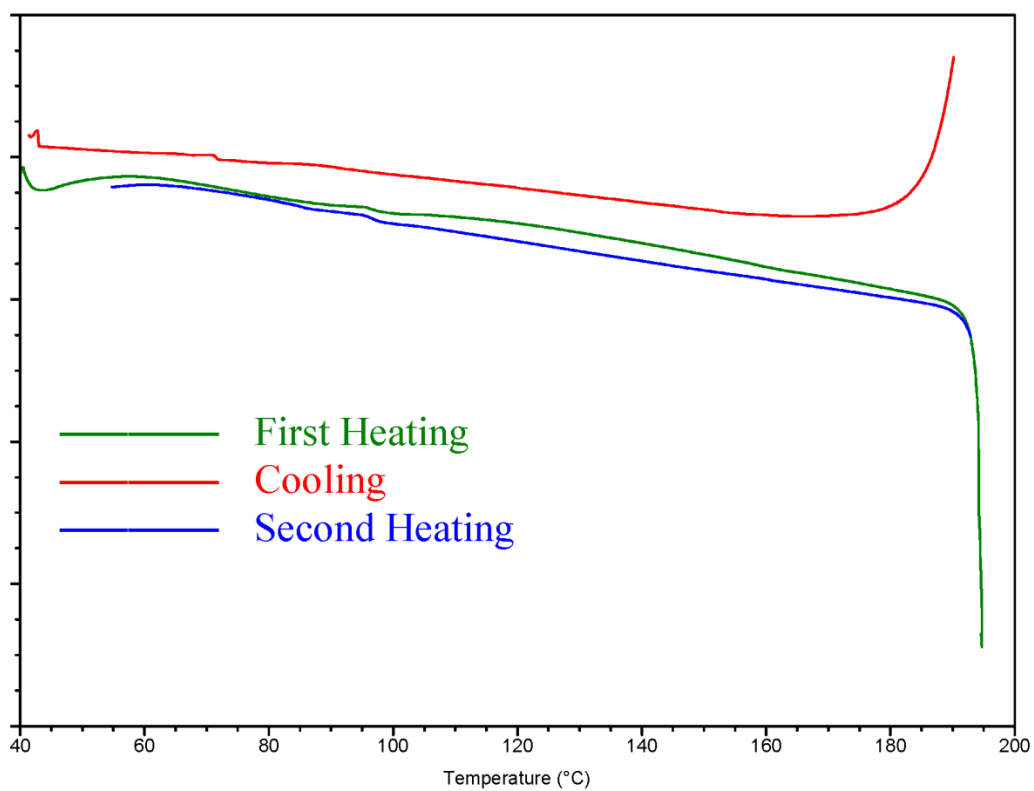


Figure 43. DSC trace of PIP₁₅Br **1e**.

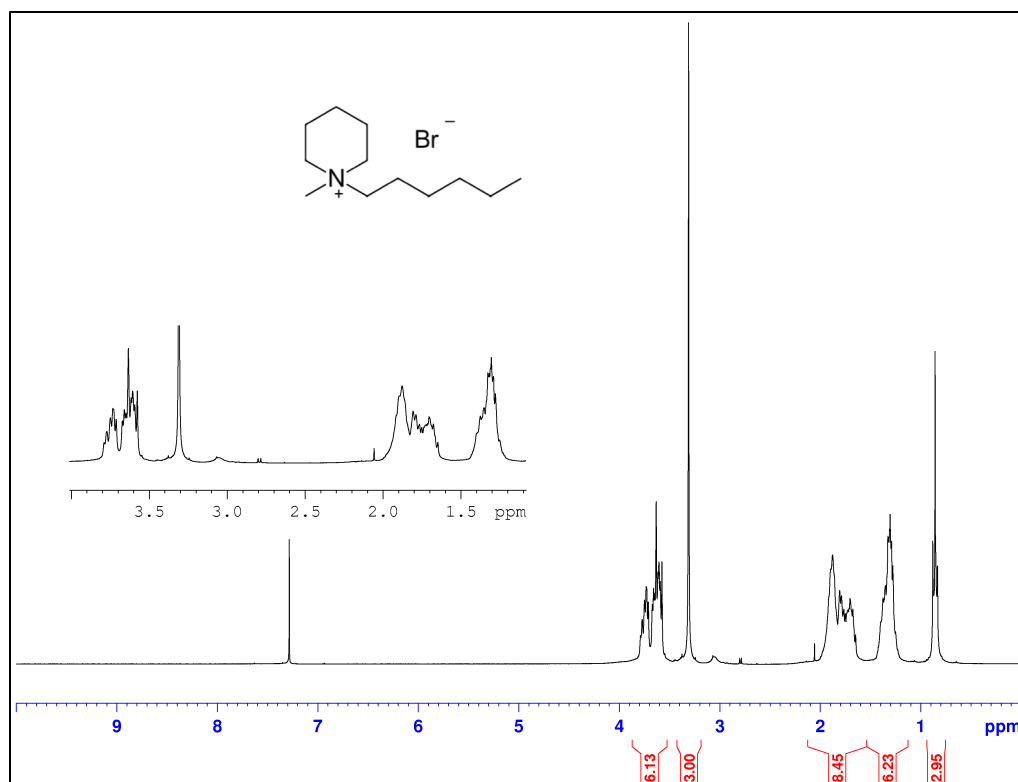


Figure 44. 300 MHz ¹H NMR spectrum (CDCl₃) of PIP₁₆Br **1f**.

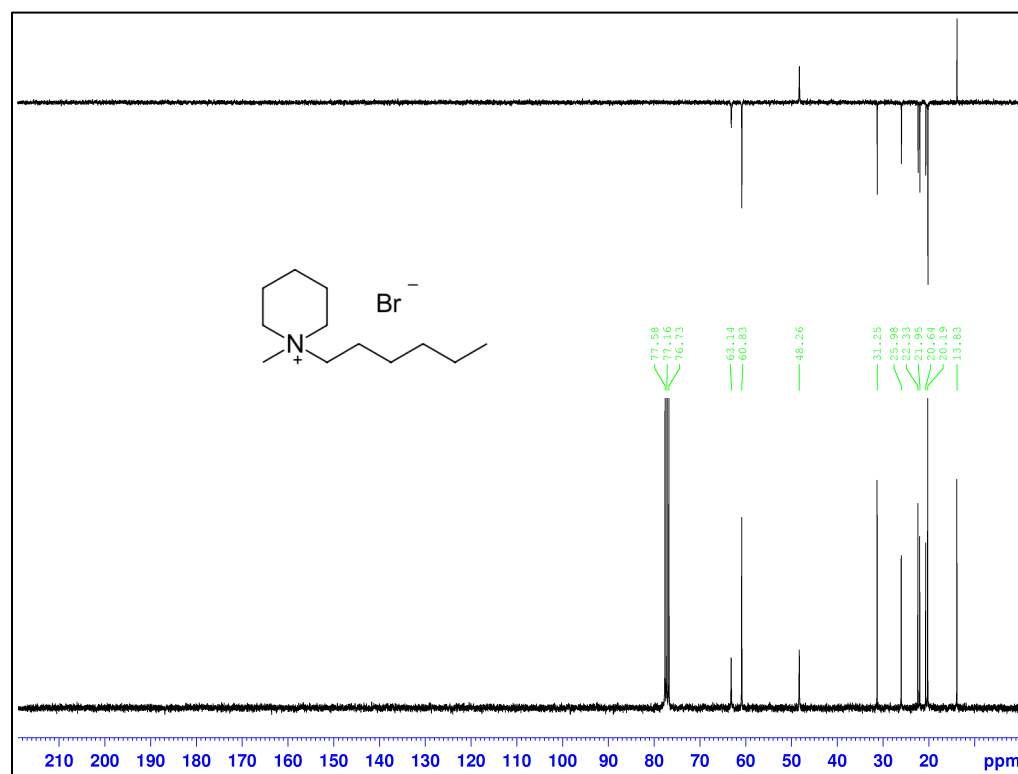


Figure 45. 75 MHz ¹³C and Dept 135 NMR spectra (CDCl₃) of PIP₁₆Br **1f**.

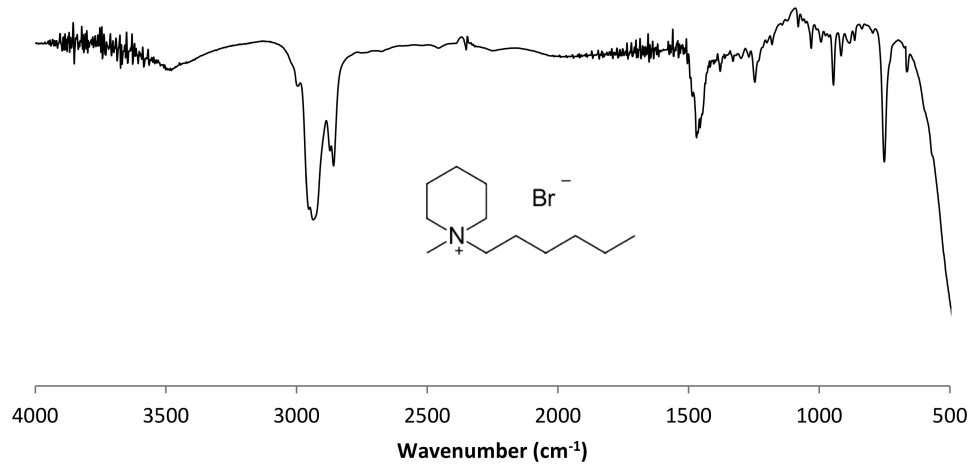


Figure 46. IR (NaCl plate) spectrum of PIP₁₆Br **1f**.

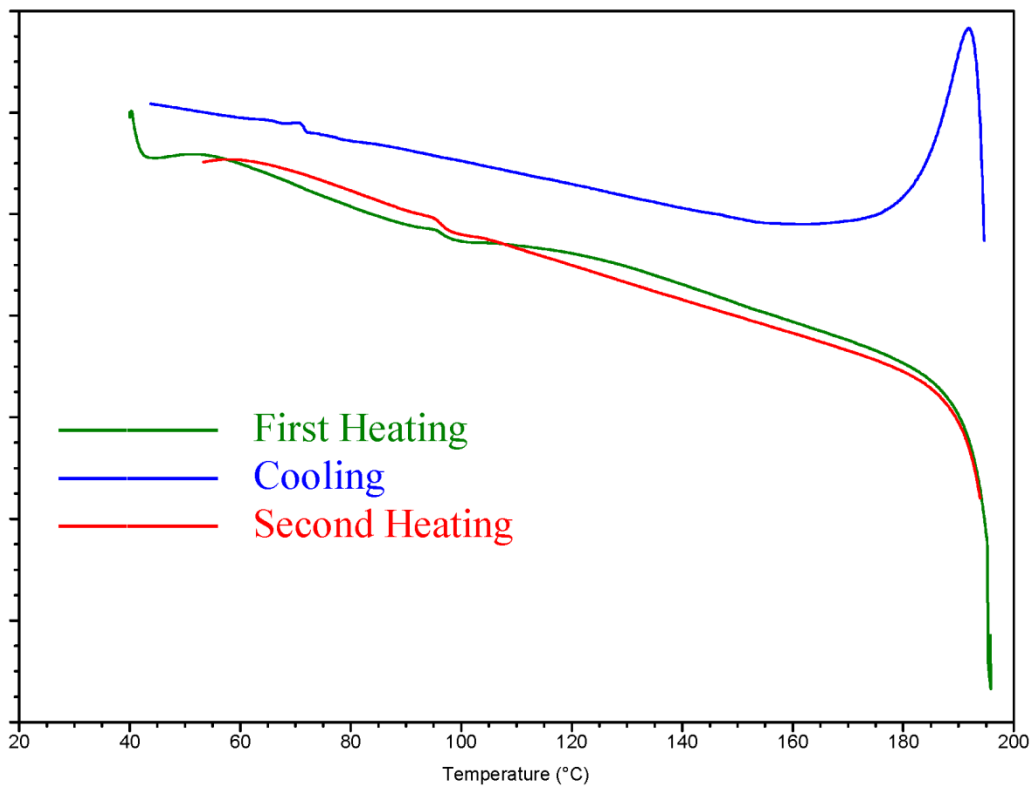


Figure 47. DSC trace of PIP₁₆Br **1f**.

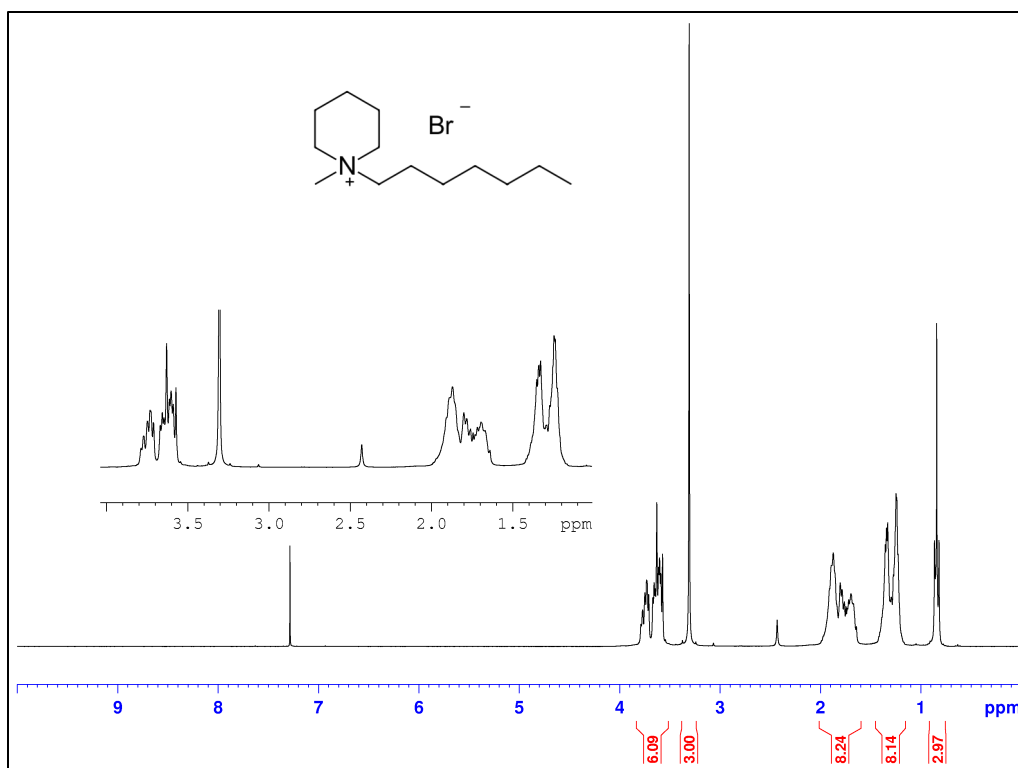


Figure 48. 300 MHz ^1H NMR spectrum (CDCl_3) of PIP₁₇Br **1g**.



Figure 49. 75 MHz ^{13}C and Dept 135 NMR spectra (CDCl_3) of PIP₁₇Br **1g**.

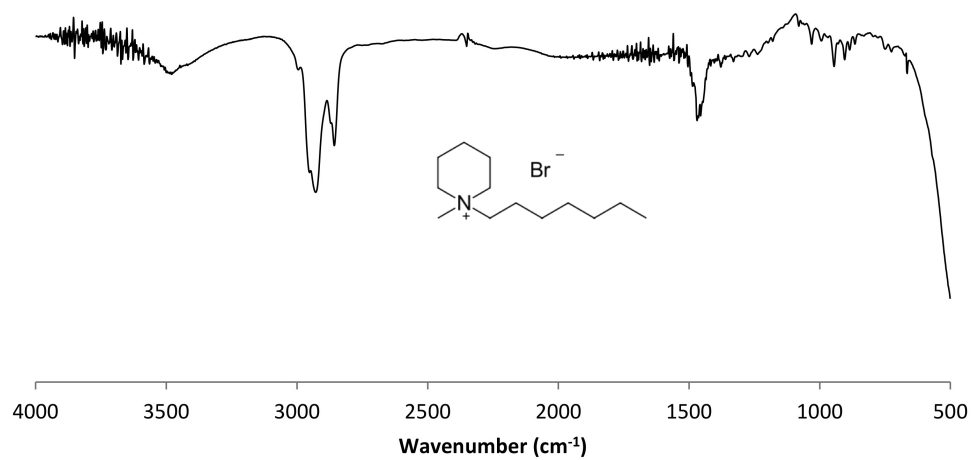


Figure 50. IR (NaCl plate) spectrum of PIP₁₇Br **1g**.

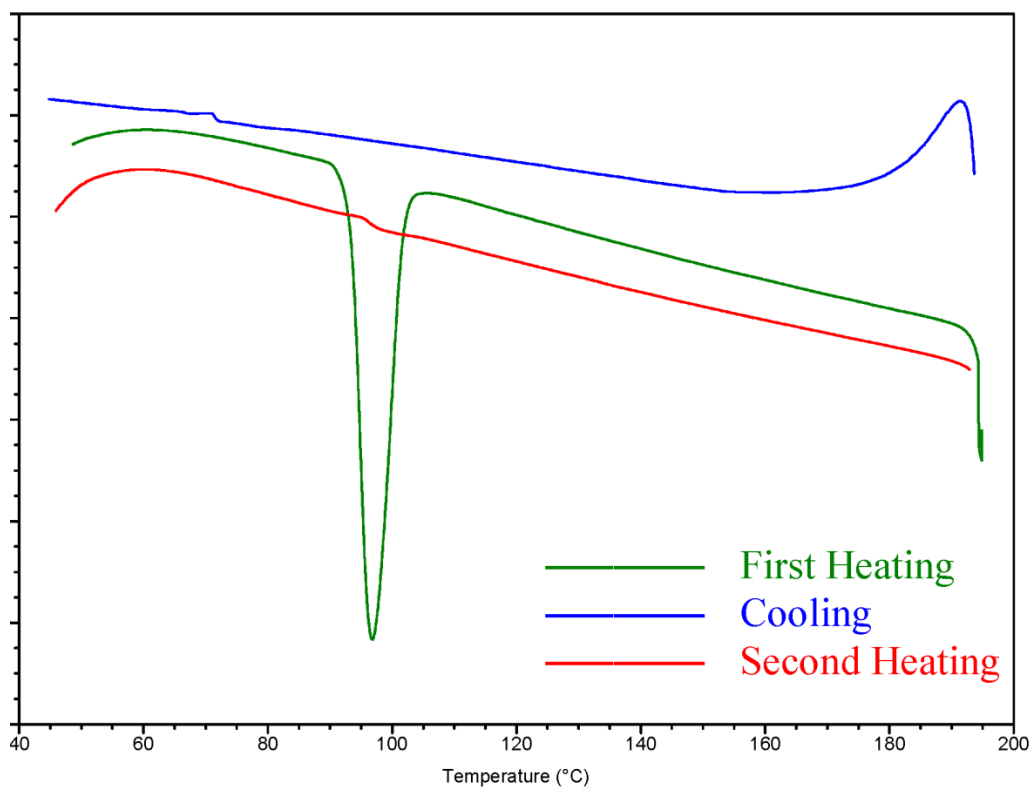


Figure 51. DSC trace of PIP₁₇Br **1g**.

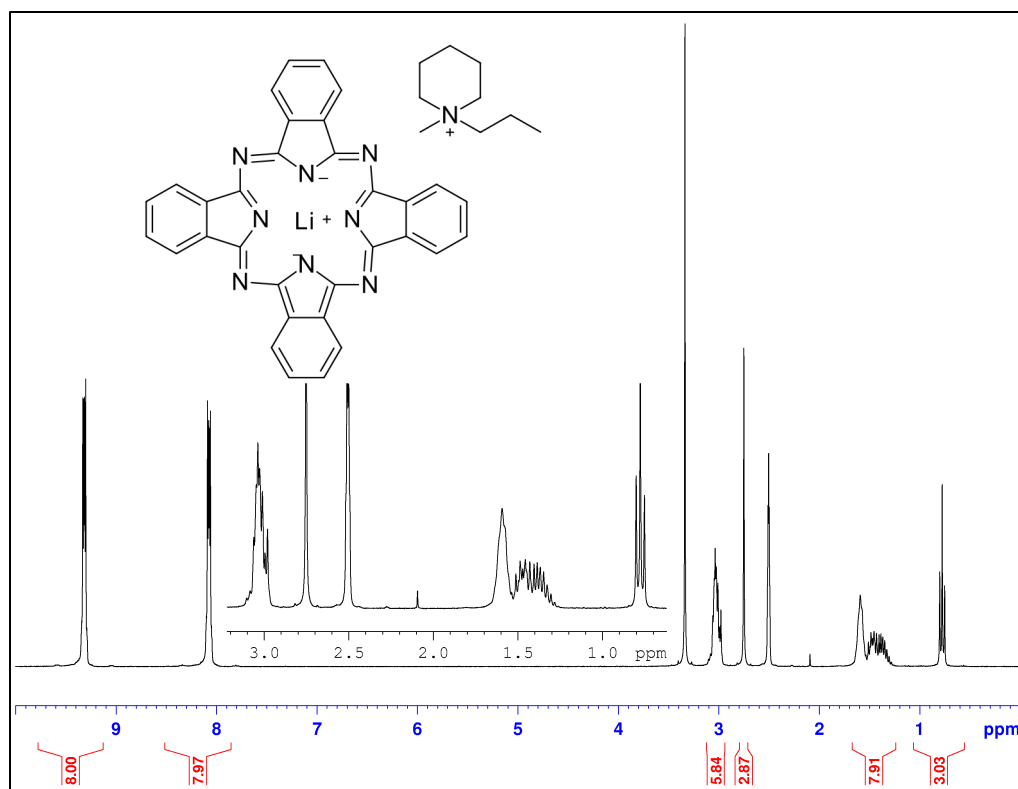


Figure 52. 300 MHz ¹H NMR spectrum (DMSO-d₆) of PIP₁₃Br LiPc 21.

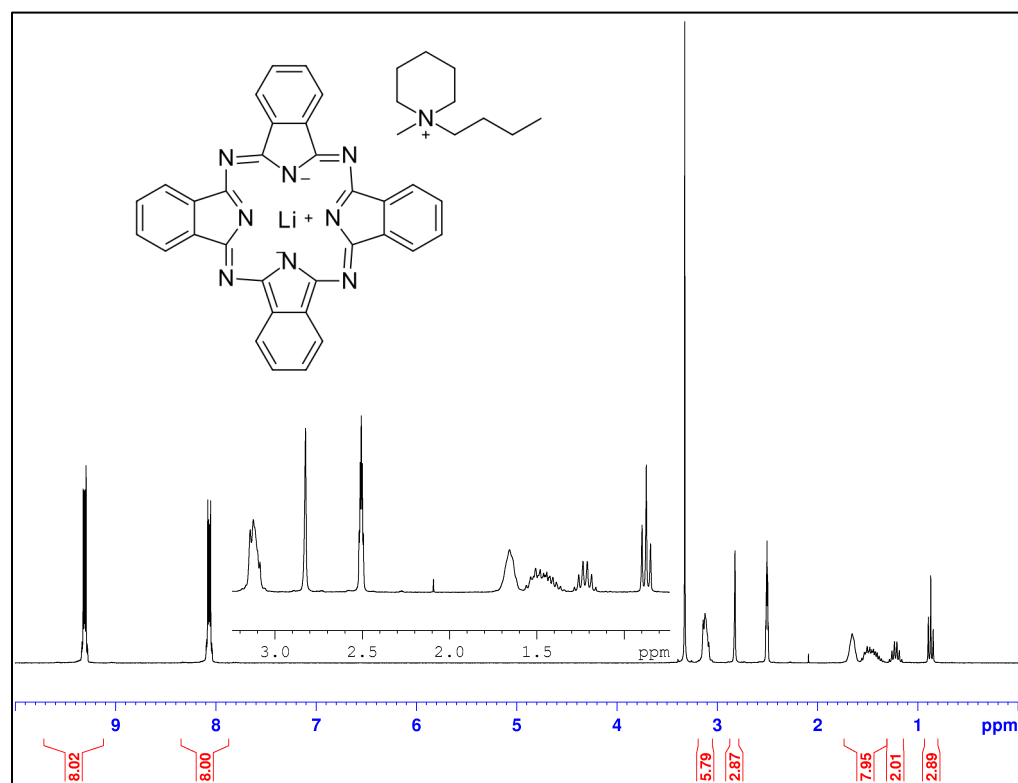


Figure 53. 300 MHz ¹H NMR spectrum (DMSO-d₆) of PIP₁₄Br LiPc 22.

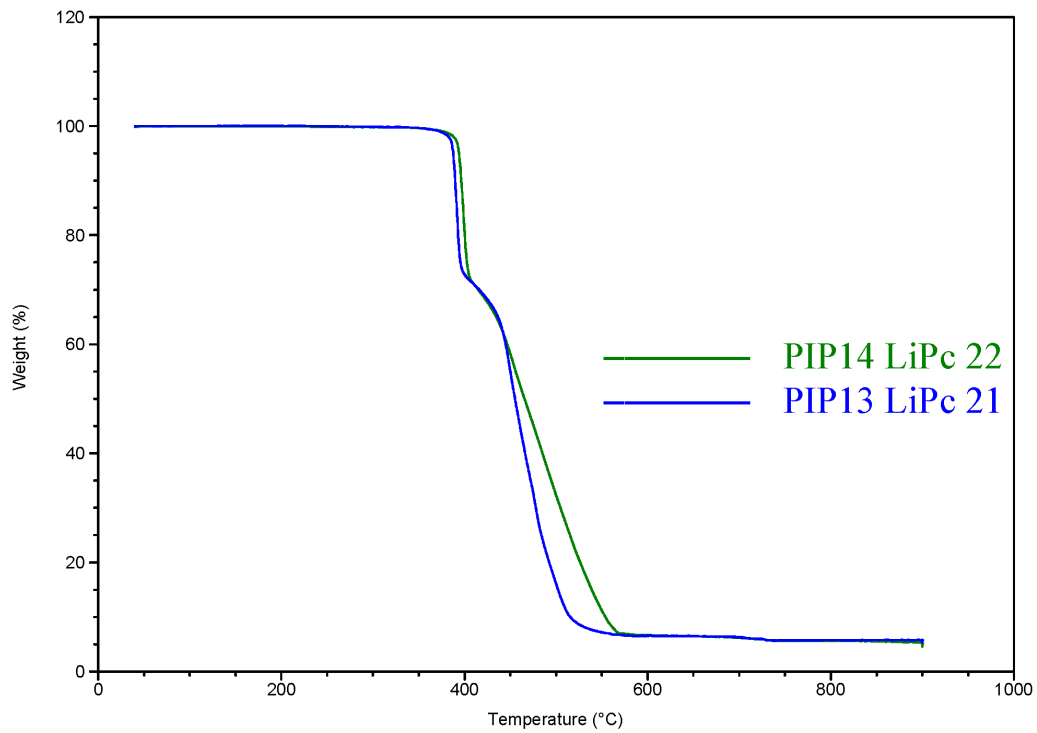


Figure 54. TGA overlay of PIP₁₃ LiPc 21 and PIP₁₄ LiPc 22.

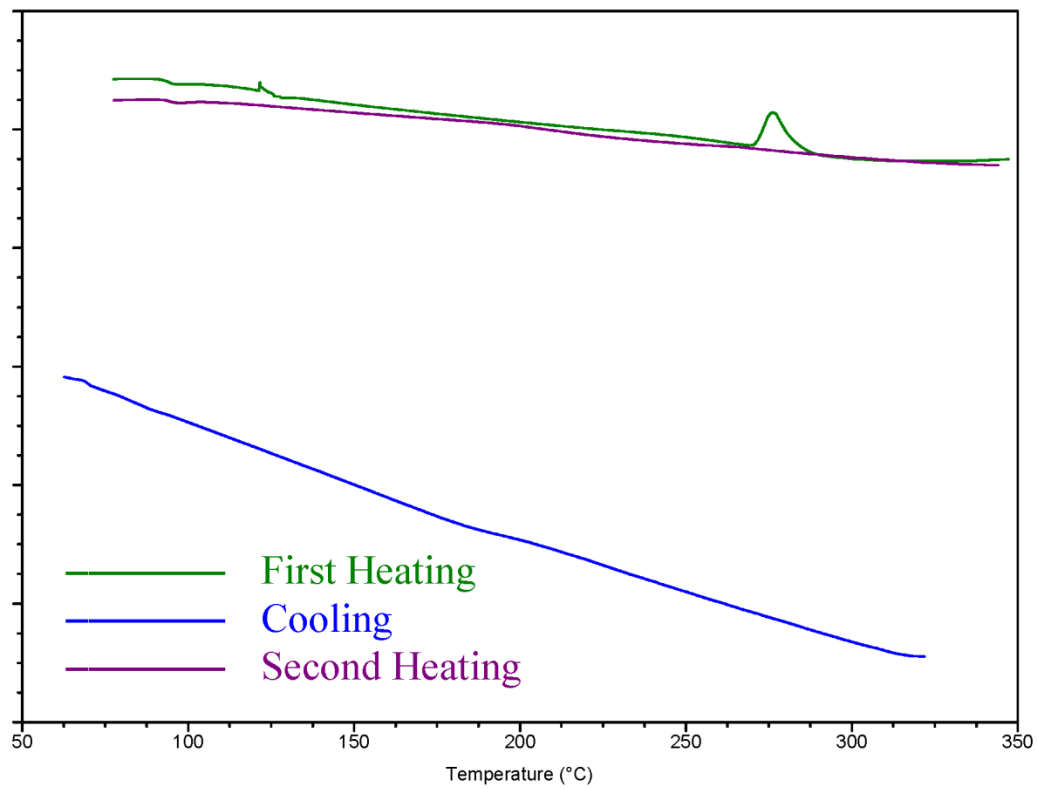


Figure 55. DSC trace of PIP₁₃ LiPc 21.

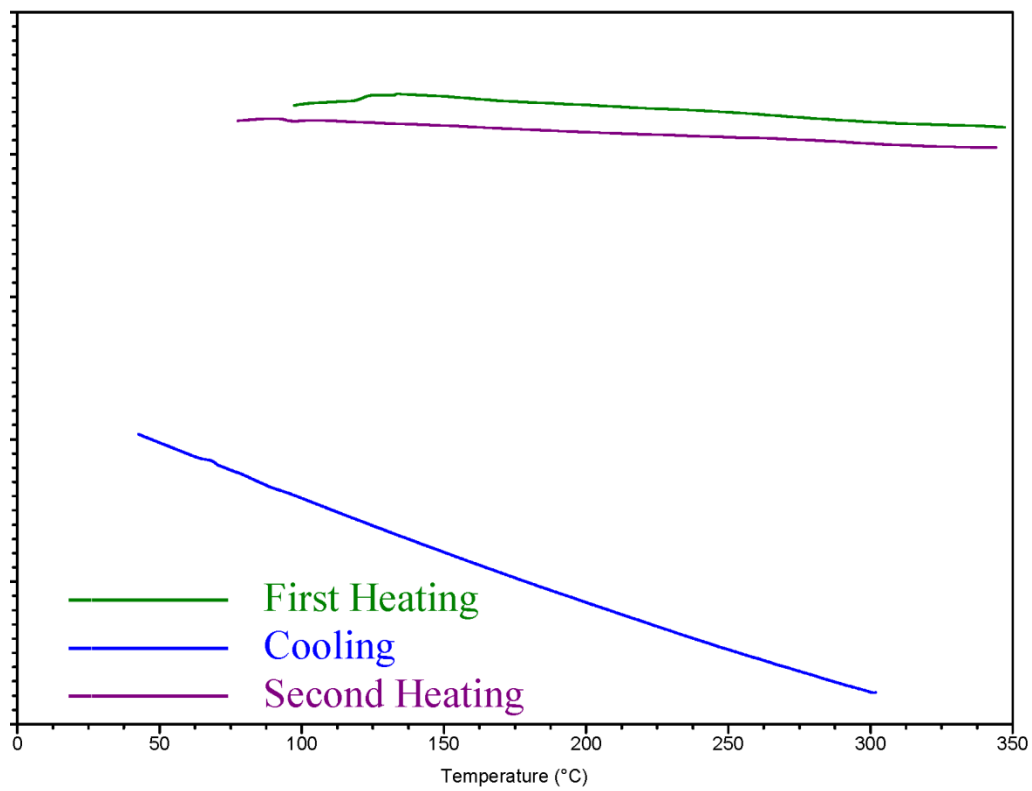


Figure 56. DSC trace of PIP₁₄ LiPc 22.

REFERENCES

1. K. R. Seddon, *J. Chem. Technol. Biotechnol.*, 68, 351, **1997**.
2. G. B. Appetecchi, S. Scaccia, C. Tizzani, F. Alessandrini, and S. Passerini, *J. Electrochem. Soc.* 153, A1685, **2006**.
3. A. Triolo, O. Russina, B. Fazio, G. B. Appetecchi, M. Carewska, and S. Passerini, *J. Chem. Phys.*, 130, 164521, **2009**.
4. K. Lava, K. Binnemans, and T. Cardinaels, *J. Phys. Chem. B.* 113, 9506-9511, **2009**.
5. Y. Zhao, X. Yue, X. Wang, D. Huang, and X. Chen, *Colloids and Surface A: Physicochem. Eng. Aspects.* 412, 90-95, **2012**.
6. H. Sakaebe, H. Matsumoto, *Electrochem. Commun.* 5, 594-598, **2003**.
7. A. Lewandowski, and A. Olejniczak, *J. of Power Sources*, 172, 487-492, **2007**.
8. X. G. Sun, and S. Dai, *Electrochimica Acta*, 55, 4618-4626, **2010**.
9. McKeown, N.B., *Phthalocyanine Materials: Sythesis, Structure and Function*. Cambridge: Cambridge University Press, **1998**.
10. Linstead, R. P., *J. Chem. Soc.*, 1016-17, **1934**.
11. Ziolo, R. F., Gunther, W. H. H., and Troup, J. M., *J. Amer. Chem. Soc.*, 103, 4629-30, **1981**.
12. Ziolo, R. F., and Extine, M., *Inorganic Chem.*, 20, 2709-11, **1981**.
13. Dandridge, A. G., Drescher, H. A. E., Thomas, J., Dyes. British Patent 322, 169 (1929)

14. Snow, a. W., Griffith, J. R., and Marullo, N. P., *Macromolecules*, 17, 1614-24, **1984**.
15. Scanlon, L. G., Lucente, L. R., Feld, W. A., Sandi, Campo D. J., Turner, A. E., Johnson C. S., and Marsh R. A., *Electrochemical Society Proceedings*, 2000-36, 326-39, **2000**.
16. Scanlon, L. G., Lucente, L. R., Feld, W. A., Sandi, G., Balbuena, P. B., Alonso, P. R., and Turner, A., *J. Electrochem. Soc.*, 151, A1338-A1343, **2004**.
17. Grossie, D. A., Feld, W. A., Scanlon, L., Sandi, G., and Wawrzak, Z., *Acta Cryst.*, E62, m827-m829, **2006**.
18. Homborg, H. and Kalz, W., *Z. Naturforsch.*, **1978**, 33b, 968-975.
19. Homborg, H. and Kalz, W., *Z. Naturforsch.*, **1978**, 33b, 1067-1071.
20. Schweiger, K., Hückstädt, H. and Homborg, H., *Z. Anorg. Allg. Chem.*, **1998**, 624, 44-50
21. Kelley, J. J., M.S. Thesis, Wright State University, August, **2008**.
22. Hart, M., M.S. Thesis, Wright State University, December, **2009**.
23. Beauchamp, A., M.S. Thesis, Wright State University, March, **2012**.

VITAE

Michael Joseph Krol Jr. was born in Rockford, IL and raised in Harvard, IL. He graduated from Harvard Community High School, in 2007. He graduated college from Loras College in Dubuque, IA, where he played two years of intercollegiate basketball. He received his Bachelor of Science in Chemistry, in 2011. He attended Wright State University as a graduate student to earn his Master of Science in Chemistry.